THICKNESS MEASUREMENT USING ION BEAM TECHNIQUES

RAMASUKUDU GABRIEL PITSOANE

Dissertation submitted in partial fulfillment of the requirements for the degree of

MASTER OF SCIENCE (APPLIED RADIATION SCIENCE AND TECHNOLOGY)

Centre of Applied Radiation Science and Technology

University of North West

Promoter: Dr. W.J. Przybylowicz, Materials Research Group, iThemba LABS, Faure

Co-promoter: Dr. E. Sideras-Haddad

JULY 2003

Acknowledgements

This work was completed with the guidance and help of a number of people to whom I would like to express my sincere gratitude:

Many thanks to:

MARST teaching staff at the University of North West.

Dr. W. Przybylowicz, my supervisor for his guidance, assistance, advice and encouragement throughout the study.

Dr. C. Theron for assistance and expertise.

K. Springhorn, C. Doyle, L. Ashworth and S.Marsh for the running of the accelerator and computer maintenance.

Z. Mabona, M. Nkosi and L. Vilakazi for assistance with the experiments at solid-state lab.

E. Mohajane, L. Senoko, Dr. D. Budka, L. Amon, M. Eisa, P. Sechogela, J. Mars, Dr. J. Mesjasz-Przybylowicz, T. Ntsoane, R. Bucher and the staff at MRG for their encouragement.

NRF, ESKOM and iThemba LABS for support.

My parents MAKWE and BAFI and also to my brothers and sisters.

My Creator to whom I am forever grateful for all the blessings.

"Modimo e re mmotileng ke sebo se se thata"

-

Abstract

Surface layer coatings, which are thin films in the range of micrometer and nanometer are of utmost importance. These layers have many applications and control processes like corrosion, friction, wearing and adhesion. Therefore the search for layers with satisfactory surface properties for different applications is needed.

Thickness measurements were evaluated in this study using PIXE in conjunction with RBS. Different samples were evaluated using both the solid-state chamber and the nuclear microprobe. The energies of 2.0 MeV alpha particles, 2.5 MeV and 3.0 MeV protons were used in this study. RBS when compared to PIXE showed low sensitivity towards light elements. The High purity Germanium detector also found it difficult to resolve peaks of elements (Magnesium and Aluminum) that were close to one another. The GeoPIXE software showed inconsistent results for all the measurements. However the results showed good agreement between the two techniques.

The overall observation of the study was that PIXE has shown its ability to measure thickness and that the inconsistency in the results from GeoPIXE software makes it difficult to trust the software for analysis of the results.

Declaration

I, the undersigned, hereby declare that the work contained in this thesis is my own original work and has not previously in its entirety or in part been submitted at any university for a degree.

Signature: P. Ntsoane

Date: 19-02-04

TABLE OF CONTENTS

List of figures

List of tables

Chapter 1

1.1 Introduction

Surface layers, which in most cases are thin films in the nanometer and micrometer range, have large influence on chemical and mechanical properties of most solids. These layers are mostly used as coatings in surface property modifications and they control processes like corrosion, friction, wearing, adhesion and fracture. Surface modification is the final step in many manufacturing processes and it is usually a technologically advanced process [Feldman and Mayer, 1986]. For example, extremely hard materials tend to be brittle (with low tolerance for impact stress) while resilient materials tend to be very soft. Steels with excellent corrosion resistance tend to have relatively low hardness. Therefore it is desirable to create materials with layers or regions with different tribological properties since most are of importance in many technological applications. The applications of thin films on these layers extend from diffusion barriers in electronics to electrical contacts and optical, decorative and wear resistant coatings [Campbell *et al* 1994]. Therefore, the development of techniques for surface modifications makes it possible for example, to manufacture drill bits with bulk strength and self resilient, but with hard surfaces to provide better cutting edges and wear resistant. In most cases, thin layer coatings are used in these modifications and the layer thickness for such coatings must be accurately known. Error in thickness measurement can lead to wrong conclusions and consequences of mistakes in the interpretation of data from analysis can be severe. Hence measurements must be as

accurate and precise as possible. Modification can be done either by addition of a hard surface layer or by tailoring the already existing layer.

1.2 Methods of thickness measurement

There are several available methods for thickness measurement which can be used within the nanometer and micrometer range and these include: profilometer, optical microscope, Scanning Electron Microscope (SEM) and Ion Beam Analysis techniques (IBA). Each method has its advantages and drawbacks. These methods are briefly discussed below and much emphasis will be on ion beam analysis described in chapter 2.

1.2.1 Optical confocal microscopy

It serves to reveal structures of objects such as micrometer-sized structures of microelectronic devices on silicon wafers. The resolution of the technique is determined by the wavelength of the light and the objective of the microscope. In this technique, one concentrates on a section in which each layer is visible. The technique works mostly in the range of 0.5 – 1000 μm and its drawback is that sufficient contrast of optical images to distinguish layers is required and that images may be blurred at certain distances [www.microscopyu.com].

1.2.2 Profilometer

This equipment measures surface profiles by scanning a mechanical stylus across the sample. A flat surface with well-defined step is required to generate a good profile step height measurement or an edge. The most commonly used method of analysis is based on dividing the roughness variation into separate wavelength bands and stating the mean square root value of roughness variation for each band. Based on the wavelength, the method can then be used to measure etch depths, deposited film thickness and surface roughness. Thickness of the range 0.2 to 1000 μm can be measured with this technique. Its drawback is that a well-defined step is required for good measurements [www.nanoscience.com].

1.2.3 Scanning Electron Microscopy

In this technique, a beam of electrons with energies up to 30 keV is focused at the surface of the specimen in the microscope and scanned across it in a pattern of parallel lines. Secondary electrons with energies of a few tenths of electron volts are emitted and also there is reflection of high-energy backscattered electrons of the primary beam. The emitted electron current is collected and amplified and variations in the resulting signal strength result in brightness variations during scanning. The resulting variation is then taken as the resolving power of the instrument and may be in the range of 0.1 nm –100 μm. Therefore one can measure depth by measuring the distance between the various bands. Lack in brightness variation can give poor results. [www.rit.edu/%7Ebekpph/sem/572_outline.html]

1.3 Objective and the scope of investigation

The study's main objective is to optimize the thickness assessment of thin films grown on matrixes based on the most suitable analytical conditions at the Material Research Group (MRG), iThemba LABS experimental facilities. This means performing measurements with the best level of accuracy using the common analytical techniques, which include spectra processing using suitable and standard analytical software adopted for Ion Beam Analysis (IBA) spectrometry. On the other hand, since similar conditions are used in many other laboratories using ion beams, this research will have a much broader use. There is also a need for improvement of procedures for thickness evaluation at MRG because so far, only the BS technique has been used and this is sometimes inadequate. An in-depth evaluation of capabilities of thickness measurement using ion beam technique other than BS has long been neglected at MRG (iThemba LABS). PIXE is being evaluated as an alternative method of thickness evaluation and compared with results obtained with backscattering spectrometry. Most modifications analysis were done with the aid of backscattering analysis [Demortier *et al*, 1990] but our study will focus on thickness evaluation of surface layer in the range of about 1μm to tenths of micrometers using PIXE in order to enhance ways for studies of surface layer modifications [Osipowicz *et al*, 1990]. The experimental techniques used in this investigation were described. The experiments done by Campbell (thickness measurement of TiN layers on steel substrate using PIXE and proton scattering) have been repeated in chapter 3 to make sure that the calibration measurements are correct before measurements were made in this research work. Results, discussion and conclusion are in chapter 4 and 5.

Chapter 2

2.1 Ion beam analysis

The understanding of the structure of atoms and atomic nuclei is based on scattering experiments. Such experiments were employed in determining the interaction of a beam of elementary particles (photons, electrons, neutrons, ions) with the atom or nucleus of a known element. When these interaction fundamentals became more understood, the scientific community then recognized the importance of the inverse process that is measuring the interactions of radiation with the targets of unknown elements. The initial motivation for these studies was basic science but the important applications of ion beams for material modification and ion beam-related analysis techniques that emerged turned the use of ion beams to great practical importance [Feldman and Mayer, 1986]. The need for these ion beam-related techniques has been mainly triggered by the development of devices like semiconductors that require ion implantation and diagnosis, methods for evaluation of crystal quality, and thin-film quality. As a result, the fields of "ion beam modifications of materials" (IBMM) and "ion beam analysis" (IBA) were established. This research fields offer many advantages owing to the different interactions of MeV ions with matter, such as differences in their rates of energy loss, atomic and nuclear excitations, elastic and inelastic scattering, nuclear reactions and channeling. Furthermore, because of the more complex stopping processes of ions in matter and information obtainable from the kinematics involved in the ion-atom collisions, vast amount of information can be drawn from beam analysis experiments.

2.2 Ion-solid interactions

The knowledge of the slowing down of ions traversing matter is of utmost importance in the analysis of materials where beams of charged particles are concerned. Ions lose kinetic energy during their passage through matter by colliding with electronic clouds or with atomic nuclei. The resultant energy transfer causes ions to slow down until they come to rest at some depth in the material. However, the atomic nuclei are so small hence a collision between an ion and a nucleus occur infrequently. Therefore most of the energy of the ion is lost in collision with the atomic electrons. This process determines the distance travelled by ions before they come to rest, which is their range in matter. The process of measuring this range is not as simple as that. The atomic density of the material has to be taken into consideration. This is due to the large variation in atomic density across the periodic table which results in different energy losses for different elements. The stopping cross-section also plays a role in energy loss. The increase in stopping cross-section results in an increase of energy loss.

The way in which MeV light ions lose energy through matter by colliding with the atomic electrons can be described using low- and high-energy regimes. In the high-energy regime, the rate of energy loss decreases with increasing ion energy. This is because the ions pass through the orbiting electron clouds faster and have less chance of colliding with them. In the low-energy regime, the energy loss increases with increasing ion energy and this is due to the slow ion velocity when compared with that of the inner electrons of the atomic nuclei.

Nuclear collisions are also important. They provide the analytical signals measured with the backscattering spectrometry. The nuclear energy loss rises towards the end of the

ion range. Therefore the nuclear energy loss of an ion creates less damage to the material being analyzed. This is also due to that when entering the material, they suffer only slight broadening hence can penetrate several microns into the specimen.

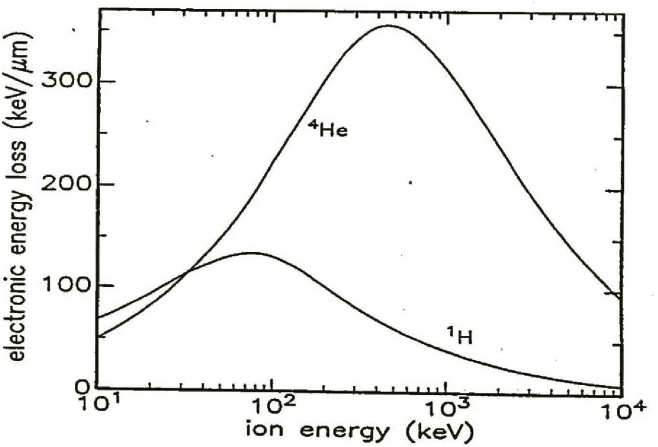

Figure 2.1. Average energy loss for 1H ions and 4He ions in amorphous silicon as a function of ion energy. [Breese *et al*, 1996]

2.2.1. Overview of techniques based on MeV ion beams

Ion beam analysis comprise a series of techniques, which among others include backscattering spectrometry also known as Rutherford backscattering (BS/RBS), particle induced X-ray emission (PIXE), nuclear reaction analysis (NRA) and elastic recoil detection analysis (ERDA). These techniques have found many applications in the field of material analysis [Breese *et al*, 1996]. The basic principles of these techniques is that charged ions in the form of accelerated beam are generated and

directed towards a certain specific material or object usually referred to as a target. Secondary radiation emitted from the beam-target interaction is then used to obtain specific information about the nature and composition of the target material. IBA depends on the detection and intensity measurement of particles and radiation that emerge from the material that is irradiated by ions. During analysis, elements can be identified based on the energy of the emergent radiation while the atomic concentration is based on the intensity of this radiation. The depth profiles can also be found from measurements based on the energy loss of ions in matter. Figure 2.2 shows RBS technique and its capability in depth profiling.

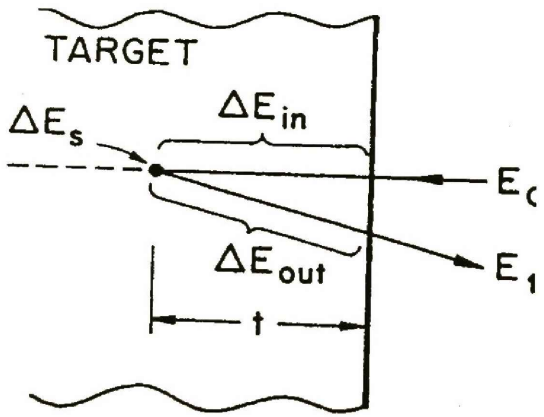

Figure 2.2 Energy loss components for a projectile that scatters fro depth t. ΔE_{in}: energy lost via electronic stopping on inward path, ΔE_s: energy lost in the elastic scattering process, ΔE_{out}: energy lost to electronic stopping on the outward path.

2.3 Backscattering Spectrometry or Rutherford Backscattering Spectrometry

Backscattering spectrometry, also known as Rutherford backscattering, is an analytical technique that has been used extensively to obtain information on the atomic composition and concentration profile of the near surface regions of materials. Compared to other ion beam techniques, it is considered to be easier, simple to understand and apply since the physical processes involved are very well understood as also is the instrumentation.

In this technique, an incident beam of mono-energetic particles impinges on the material to be studied. During collision, energy is transferred from incoming projectile particles to stationery target atoms and the projectile backscatters into a suitable detector-analysis system, which measures the energy of the backscattered particles. The reduction in energy of the backscattered particle will then depend on the masses of incident and target atoms and since the charged particles scatter from different nuclei in distinct and well-understood manner this is used to provide information on the nature of the target atoms as well as their distribution in depth[Feldman and Mayer, 1986]. Based on this, masses of different elements and isotopes can be distinguished. Figure 2.3 shows a schematic of experimental setup of the backscattering spectrometry.

Backscattering spectrometry is also a non-destructive (as long as the beam dose is kept relatively low) depth profiling technique used for determination of surface and near surface layers (Räisänen et al 1990). Thickness in the range of nanometers to micrometers can be determined and in most cases alpha particles of energy in the

range 1-3 mega-electron volt is used. The ion-solid interaction at this energy range can be considered as Rutherford backscattering or central force scattering. The scattering cross section for central force scattering was originally derived by Rutherford and hence the name of this technique. Depth profiling in backscattering spectrometry involves 3 main concepts, each of which relates to an analytical capability of the method.

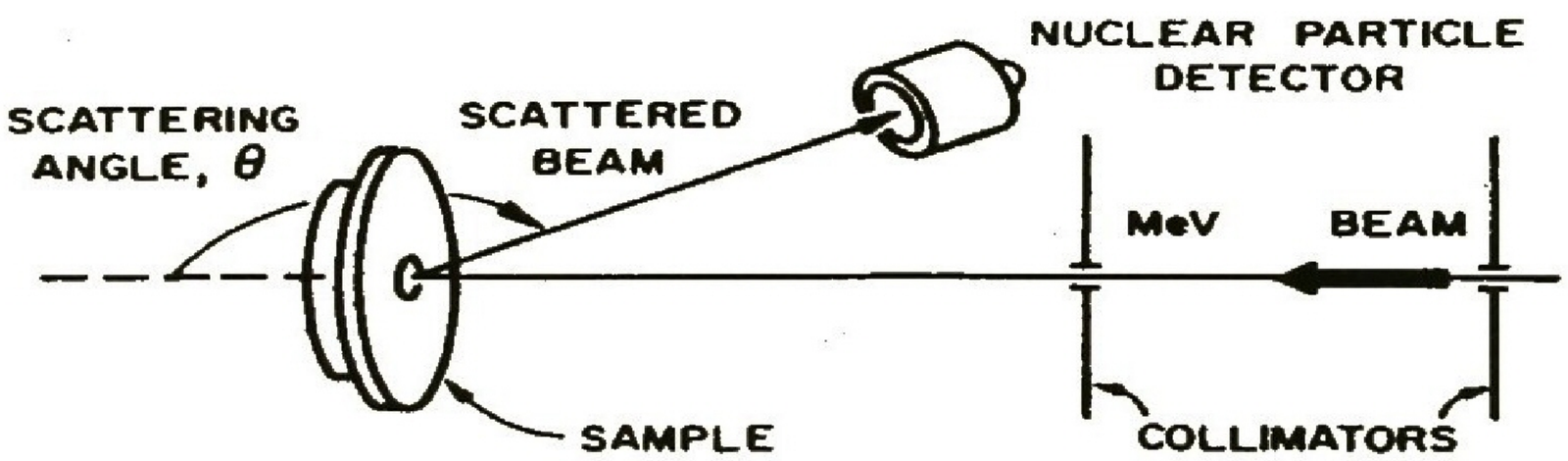

Figure 2.3 A schematic of the experimental setup for backscattering spectrometry. [Feldman and Mayer, 1986]

2.3.1 Concepts of backscattering spectrometry

The three most important concepts in backscattering spectrometry are:

a) kinematic factor K (mass analysis);

b) differential scattering cross section (quantitative analysis);

c) the energy loss of a particle (depth analysis).

2.3.1.1. Kinematic factor

Consider an elastic collision between a moving particle (projectile) with stationery particle (target). The masses of the projectile and the target remain constant after the collision. The ratio of the projectile velocity after collision to the initial velocity of the projectile is called the kinematic factor, K, and is given by:

$$K = \frac{E_1}{E_0} = \left[\frac{M_1 \cos\theta + (M_2^{\,2} - M_1^{\,2} \sin^2\theta)^{1/2}}{M_2 + M_1} \right]^2$$

where E_0 and E_1 are energies before and after collision, M_1 the projectile while M_2 is the target and theta θ the scattering angle [Feldman and Mayer, 1996]. The above equation shows that the kinematic factor depends only on the ratio of the masses of the projectile, the target and the scattering angle. Figure 2.4 shows a scattering angle.

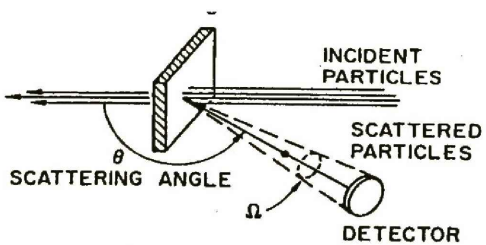

Figure 2.4 An experiment setup showing the scattering angle. [Feldman and Mayer, 1986]

2.3.1.2. Scattering cross-section

Collisions between the target and the projectile do not occur frequently and again, not all collisions result in a measurable event. The probability that a collision will occur and that a measurable event will take place at a specific angle depends on the number of particles that hit the target. The scattering cross-section is defined by

$$\sigma(\theta)=\left[\frac{Z_1 Z_2 e^2}{4E}\right]^2 \frac{4}{\sin^4\theta} \frac{\left(\left\{1-\left[(M_1/M_2)\sin\theta\right]^2\right\}^{1/2}+\cos\theta\right)^2}{\left\{1-\left[(M_1/M_2)\sin\theta\right]^2\right\}^{1/2}}$$

where E is the energy, Z_1 and Z_2 the atomic numbers of a projectile and target atoms, e^2 the electronic charge, M_1 and M_2 the masses of incoming particle and target nucleus [Feldman and Mayer, 1996]. The equation shows that the scattering cross-section is inversely proportional to the energy of the projectile. Figure 2.5 shows the concept of cross-section.

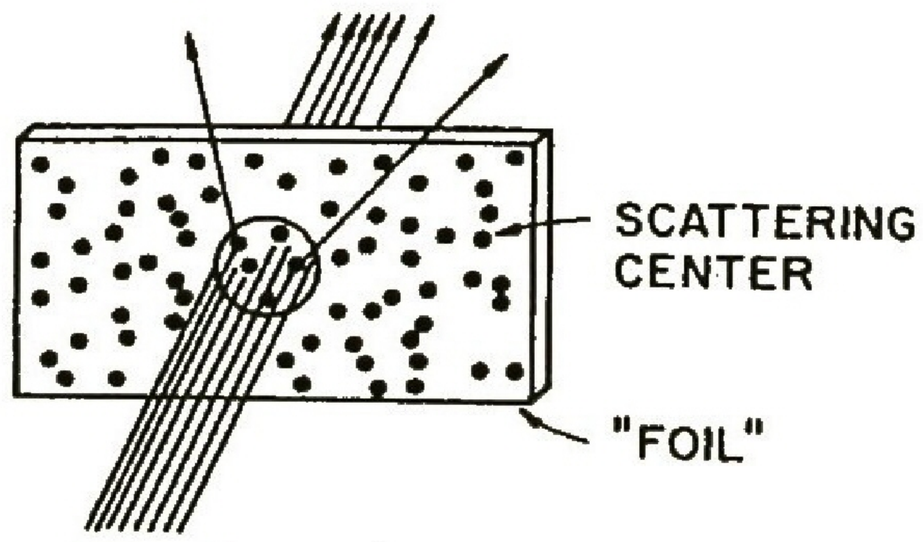

Figure 2.5 Illustration of the concept of cross-section. From knowledge of detection efficiency for measuring the emergent radiation containing the signature of the transition, the number of atoms and ultimately the target composition can be found. [Feldman and Mayer, 1986]

2.3.1.3. Energy loss factor

The particle loses energy as it penetrates through the target. The particle can then undergo an elastic collision and change its trajectory into an outward direction. During its outward path, it looses energy until it emerges from the target. By measuring this energy loss, the depth to which the particle has penetrated can be determined. The energy loss is defined by the following equation:

$$\Delta E = \Delta t\left(K\frac{dE}{dx}\Big|_{in} + \frac{1}{|\cos\theta|}\frac{dE}{dx}\Big|_{out}\right) = \Delta t[S]$$

where ΔE is the energy loss, Δt the depth, K the kinematic factor and [S] the backscattering energy loss (the amount of energy lost per distance traversed) factor [Feldman and Mayer, 1996].

Based on the above discussed concepts it was determined that the technique is not suitable for the analysis of layers whose elements have an atomic weight close to that of the backing material especially when the element in the thin layer is lighter than that of the substrate (Havránek *et al*, 1990). It is also difficult to resolve layers that have heavy elements with atomic numbers close to each other and that lighter elements on top of a heavy substrate may not be easily detected and that technique is limited to a certain range when thickness measurement is concerned. Therefore an alternative

method will be of great importance if one wants to measure thickness up to a certain range [Havranek *et al*, 1990].

2.3.2 RBS analysis

For Rutherford Backscattering Spectrometry (RBS), the information in the spectrum is usually used to establish the thickness and the composition of the layers in the sample. For simple spectra, it is sufficient to measure peak heights, areas, or widths and follow simple procedures to determine these quantities. In the analysis of complex spectra, computer program, which generate theoretical spectra based on the described sample, is used. The RUMP RBS simulation package has proven to be of invaluable assistance in the analysis of standard RBS. The technique involves the viewing of an overlay of a theoretical spectrum with the experimental one, and modification of parameters until an adequate fit is achieved (Climent-Font *et al*; Doolittle 1986). There are several factors that can modify the shape of an RBS spectrum concerning its matrix scattering height. These factors include: channeling, pile-up effects, plural and multiple scattering and stopping power values. Channeling effects are quite often present in RBS spectra meant to be random ones despite the precaution of tilting the sample. In this instance the experimental yield of the RBS spectrum is often decreased as compared to the computer code simulated. However, there are also special cases where channeling can give higher yields. That is when the incident angle is slightly larger than the critical angle. Therefore the experimental yields can often be explained based on channeling. Modifications of the shape of the spectra can also be due to the presence of pileups. The presence of pileup effects is usually indicated by the appearance of the energy tail

beyond the surface position energy in the spectrum. Based on the count rate, the mismatches between the simulation and the experiment can be explained.

The effects of the multiple and plural scattering also are taken into consideration when simulations are done. These effects are more important at low energies, mostly less than 0.5 MeV, where the scattering cross section is high. The backscattered yield can be increased due to this effect. Therefore it is only at this low energy part of the spectrum that can be attributed to plural and multiple scattering.

The stopping powers can also affect the simulation process. Inaccurate values of stopping power under certain conditions can leads to systematic error of the order of 10% and even higher. Therefore correct stopping power is essential for good fits in simulation.

2.4 PIXE (Particle Induced X-ray Emission)

The interaction of MeV energy ions with target material leads to the ionization of target atoms and the subsequent emission of X-rays with energies that provide characteristic signatures of the target atoms. The process of proton energy loss and X-ray absorption within the target and the X-ray detector enables the direct modeling of X-ray production. This provides a quantitative relationship between the detected yield of characteristic X-rays and elemental concentration within the target. This is the foundation of a technique called particle induced X-ray emission.

PIXE is an analytical technique in which X-ray emission is used for elemental identification and quantification. It has some distinct advantages as compared to other

techniques. Its major features are that it is multi-elemental (in principle, elements from Boron to Uranium can be measured), has high sensitivity (detection limits can go down to parts-per-million) (Ahmed *et al* 1997) and that it has the ability to analyze small amounts of material [Jakšić *et al*, 1989]. It is generally considered a non-destructive technique.

2.4.1 Basic principles

When a charged particle moves through a material, it loses energy primarily by exciting electrons in the atoms it passes by. Electrons in the inner shells of the atom (predominantly the K and L shells) are given enough energy to cause them to be ejected, resulting in an unstable electron configuration in the atom. The electrons from the outer shells in the atom then "drop down" to fill these vacancies, and by doing so, they give off excess energy in the form of X-rays (figure 2.6). The X-rays are then detected and the pulses from the detector are amplified and finally registered in the pulse height analyzer (Tapper *et al* 1994).

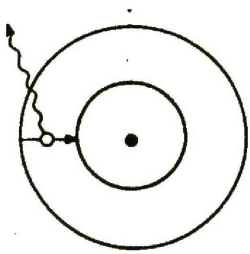

Figure 2.6 X-ray emissions as it occurs in PIXE process. [Feldman and Mayer 1986]

Since PIXE spectrum is usually quite complicated, with many peaks, some of them overlapping, a computer is used for its deconvolution. The number of pulses in each peak, which is the measure of the concentration of the corresponding element in the specimen, is calculated. By measuring intensities of characteristic X-ray lines one can determine concentration of almost all elements in the sample down to approximately 1 parts-per-million (ppm) [Johansson *et al*, 1995]. An important advantage of PIXE is that specimen of many different types can be analyzed. The most common case is in thin specimen. Thin in this context means that the accelerated particles loose only a small part of their energy when passing through the specimen. That is the energy loss is small and can therefore be neglected. This means that the excitation energy is well defined and that there is little absorption of the emitted X-rays in the specimen, which simplifies the calculations of X-ray yield. PIXE has also a high resolving power. Some components have roughly the same energy, for example $K_{\alpha 1}$ and $K_{\alpha 2}$ so they appear as a single peak in the spectrum. However, this is not the case with PIXE. In a PIXE spectrum the elements give two resolved peaks, which are K_{α} and K_{β}. The effective detection of the K X-rays can be obtained in the interval $11 < Z < 50$ and of the L X-rays for $Z > 50$. PIXE also creates less damage to the specimen. This is due to slight broadening suffered by a proton beam when entering a specimen as compared to an electron beam. Therefore based on these, protons can penetrate specimen deeper than electron beams. Figure 2.7 shows a PIXE experiment setup at the iThemba LABS microprobe chamber.

The use of PIXE in material research took a major step forward after it was realized it could be used as a depth profiling technique. Although it was viewed as a poor depth profiling technique, several studies and publications came up with something different.

Work by Demortier and others (1990), proved that PIXE is a good depth profiling technique. The work showed that thickness of up to a few tenths of micrometer could be measured. This is true because it is at this range of depth where protons can induce X-rays [Brissaud *et al*, 1985]. Therefore PIXE can be a rapid and accurate method for measurement of surface layers that are thicker than those measured by backscattering. In most cases thickness is measured based on peak ratios of characteristic lines of the surface element or the substrate. The range of thickness differs from element to element depending on the X-ray energy and the X-ray line used [Demortier *et al*, 1990]. Taking advantage of a limited thickness evaluation by other methods, PIXE was seen as an alternative and best technique for thickness measurement involving layers of thickness in the range 1-30 μm [Demortier *et al*, 1990].

2.4.2 Some aspects of PIXE quantitative analysis

a) detector-target distance
b) pile-up rejection system
c) beam on-demand deflection
d) secondary electron suppression

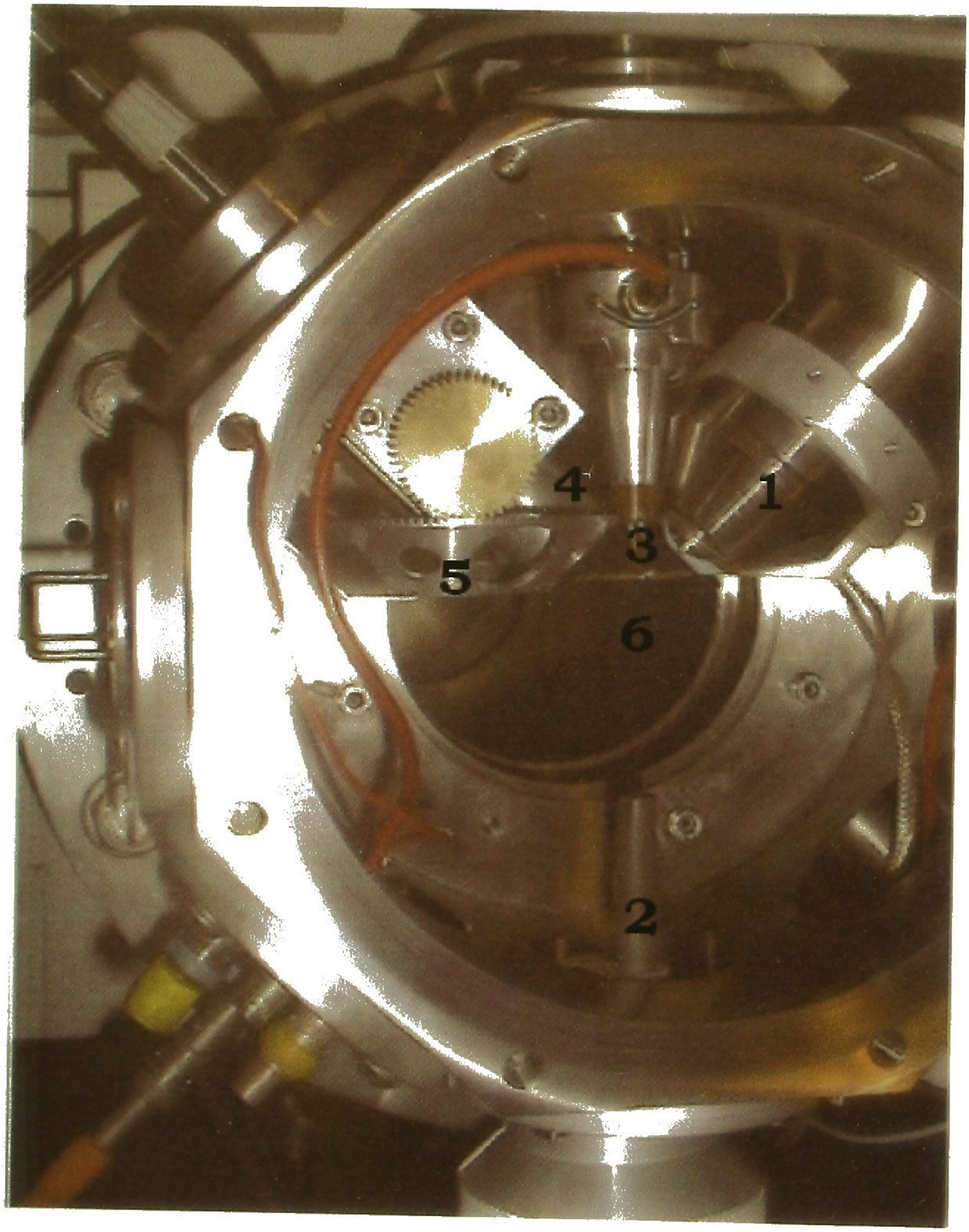

Figure 2.7 PIXE experimental setup in the microprobe chamber, Materials Research Group, iThemba LABS. (1) optical microscope, (2) Faraday cup, (3) electron suppressor, (4) PIXE detector, (5) filter wheel, (6) position of a target

2.4.2.1 Detector-Target distance

The distance between the detector and the target is of utmost importance in PIXE. X-rays scatter at different angles from the target, so if the distance between the target and the detector is increased, a certain portion of the X-rays won't be detected. This is due to fact that as the distance increases, the solid angle becomes smaller and less X-rays are detected. This is shown in figure 2.8. Therefore for a more efficient detection system, the target-detector distance should be minimal.

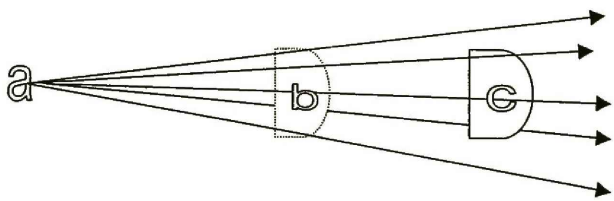

Figure 2.8 The figure shows how the detector-target distance influences the detection levels where (a) is the target, (b) and (c) is the detector at different distances.

2.4.2.2 Pile-up rejection system

Pile-ups are due to high counting rates. Pair of X-ray events that fall within the resolving time of the electronic system are summed to produce an apparent single event. This event is translated into an artifact signal positioned to the right of the characteristic peaks of a given element at more than twice the event energy (keV). This causes spectral distortion. Fast electronics, pile-up rejection system and small count rates can be used to minimize pile-ups (Amsel *et al*, 1992). A beam on demand system may be used to control the pile-up rejection when medium to high-count rates are used [Johansson *et al*, 1995].

2.4.2.3 Beam on demand deflection

One of the best ways to minimize the dead time and pile-ups is by using an on-demand beam deflector. The beam on demand system is based on a pair of electrostatic plates that are maintained at equal voltage, so in normal conditions the beam passes undeflected between them. When the detector registers relatively high count rate of X-rays, its preamplifier triggers fast-acting circuitry to remove the voltage from one plate, hence an electric field is established between the plates and the beam is deflected off the specimen. The deflection does not only minimize damage to the specimen, it eliminates dead time correction because the beam is held off the specimen until all the processing of a given pulse is complete and this lowers the intensity of pile-ups [Johansson *et al*, 1995].

2.4.2.4 Secondary electron suppression

The lowest energy X-rays tend to give the greatest yield and for these the detection limit depends mainly on secondary electrons bresstrahlung. Therefore, secondary electrons need to be suppressed since they contribute to most of the background. The electron suppression at iThemba LABS nuclear microprobe is in the form of a copper ring at – 1500 V in front of the sample. The negative voltage repels the electrons and at the same time reduces the background [Campbell and Cookson 1984] [Prozesky *et al*, 1995].

2.4.3 GUPIX, H-value and Geo-PIXE

The introduction of software packages GUPIX and GeoPIXE was specifically for PIXE spectra data analysis. Both use extensive data libraries and have proved to be reliable and accurate. GUPIX determines the intensities of characteristic X-ray peaks in a PIXE spectrum by fitting a model spectrum to the measured one using the nonlinear least squares technique. The model spectrum is constructed using a database of K, L and (as for now) M X-ray energies and relative line intensities, and the latter are modified to reflect the effects of detector efficiency, absorber effects and matrix effects. The matrix effects in turn are computed using a database of proton ionization cross-sections and stopping power, and X-ray mass attenuation coefficients. The continuous background, however, is not modeled and so the model spectrum contains only characteristic X-ray contributions. The continuous background is dealt with by applying a filter that reduces

the background to zero levels (Maxwell *et al*, 1995). GUPIX can handle thin, intermediate and thick samples. (Maxwell *et al*, 1989). It can be run either in a manual or in the batch mode and is a convenient choice for off-line (after measurements) deconvolution (Campbell *et al*, 2000).

The H-value is the product of the geometric solid angle of the X-ray detector and any systematic normalization factor present in the charge integration system. The H-value should be the same, regardless of whatever element is used as a standard. However, this only applies if the database has perfect accuracy and if the detector and absorber characteristics are perfectly known. In practice when a well characterized detector is used the H-value remain constant for K X-rays from the elements in the range $20 < Z < 50$ when the theoretical K database is used in GUPIX. Any imperfections in the database, the detector or absorber characterization leads to differences in H-value. The measured H-value is then entered into GUPIX for analysis of specimen (Campbell *et al*, 2000).

The GeoPIXE code has been developed for more specific applications, mainly for trace element analysis of mineral grains using a PIXE micro-probe. It uses the method of least squares to fit the background parameters, which is the usual approach in PIXE programs. One major advantage of the package is the dynamic analysis capability of on-line semi-quantitative analysis of spectra and on-line elemental mapping. The on-line semi-quantitative analysis capability enhances the identification of areas of interest on specimen where localization is difficult using a more primitive technique such as total X-ray map of that area. That is if the non-linear parameters describing detector characteristics such as energy calibration, peak width and tailing, have been determined in a preliminary fit, then the remaining linear parameters representing major-line peak-

areas and one representing the background intensity, can be found by solving the matrix equation. The on-line maps are presented in ppm-nC units whereas the final ones are quantitative and presented in ppm. (Prozesky *et al*, 1995; Ryan *et al*, 1990, 1990 (b)).

The challenge to tackle the imaging and analysis of complex samples mainly geological, led to the further development of Geo-PIXE software package (GeoPIXE II). This package uses the established methods of GeoPIXE for spectrum fitting and yield calculation for multi-layered samples. In these code, the energy, thickness, matrix composition are of importance. Once these parameters are specified, the program calculates the yields and gives concentration of the elements. The main features of this package are that quantitative concentration information such as average concentrations of elements in regions of arbitrary shape can be extracted. Unwanted areas can be removed from a selected area, for example in order to remove the effects of cracks in a mineral grain. In addition, projection of extracted concentration data onto a selected line across a sample permits a line profile to be extracted and displayed as element concentration histogram against distance (Ryan *et al* 2002).

The advantages of GUPIX and GeoPIXE are that no assumption needs to be made regarding the analytical form of the background, and the number of parameters involved in the least squares fitting is reduced, thus increasing the deconvolution speed. (Ryan *et al*, 1990; Ryan *et al*, 1990(b), Campbell *et al*, 2000).

The GUPIX code consists of routines for iteration of matrix composition and also thickness of each layer. The thickness iteration routine was chosen for our study. In this routine, the user is prompted for several parameters. These include information on the number of layer, beam-target-detector geometry, the incident ion type and energy. The

user is then asked to supply the list of visible elements and identify which layer they belong to. The details of the invisible elements (whose X-rays do not show up in the spectrum) are supplied. Then the layer thickness iteration is performed. In the first option, the exit proton energy of the layer is varied until the total concentration of the calculated matrix elements of the surface layer converges to one. If the calculated total concentration exceeds one, the proton energy is lowered towards zero and if it is less than one, the proton exit energy is raised towards the entrance energy. If the total calculated concentration exceeds one even if the layer exit proton energy goes to zero, the this signals that the it is impossible to make the layer thick enough with the given incident proton energy, H, charge etc to obtain convergence. In the second option, the exit proton energy of the layer is varied until the total concentration of the matrix elements of the substrate converges to one. In these options, the first method (iterate surface layer concentration to one) relies upon the X-ray production of cross sections of the upper layer elements within the matrix whereas the second method relies on the substrate X-rays. Thickness measurement in GeoPIXE is different from GUPIX. In this code, the parameters such as energy, number of layers composition and thickness are put into the system. The code then calculates the elemental concentration based on the parameters. Based on the concentration found, one can deduce whether the thickness calculated was wrong or right.

2.5. Nuclear Microprobe

Nuclear microprobe is one of the most versatile of the many research tools available for analysis techniques. It has been used in research studies since the early 1970's. The

ability of MeV ions to penetrate through surface layers on a sample with little scattering and to focus the ion beam to a probe size smaller than one micrometer is what gives the nuclear microprobe its analytical power (Breese *et al*, 1996). It is an established analytical instrument with applications in fields as diverse as biology, medicine, geochemistry, metallurgy, solid-state physics and archaeology and is mostly used for determination of minor and trace elements [Watt & Grime, 1987]. It allows measurements with spatial resolution in the order of 1μm and minimum detection limits down to few parts per million (ppm) by weight, with excellent scanning capabilities.

2.5.1 Nuclear microprobe facility at iThemba LABS

The important components of a nuclear microprobe are the accelerator, the beam line, the collimators, the sample chamber and detectors, the scanning system, and the data acquisition and analysis system. A schematic of the iThemba LABS nuclear microprobe is shown in Fig.2.9 with all beam optics features. In the beam line, the collimators limit the divergence of the beam, resize and focus the beam. The collimated beam then enters the sample chamber. Figure 2.4 shows a sample chamber configuration (with the lid removed) and the location of the most common detectors used to measure the signals from PIXE and backscattering. The chamber is a complicated part of the nuclear microprobe system. This is because samples with a very wide range of characteristics must be accommodated, as well as several detectors for the radiation and particles produced from the sample. The geometry of the detection system may range from the

detection of transmitted ions through thin samples, to the detection of photons at backward angles from thick samples.

The microprobe lid is equipped with a computer-controlled motor that allows the control of the target ladder in the X-, Y-, and Z- directions. A permanent set of standards has been mounted on the target ladder and the positions of these standards are stored in the computer memory to ease the calibration process. The vacuum is better than 10^{-4} torr with a turbo-molecular pump backed by a roughing pump. The optical microscope is used to provide information during focusing of the beam and to locate sample features. The chamber is configured for many different measurements but in practice only those detectors relevant to a particular measurement are in the chamber, allowing them to be located at their optimum positions [Breese *et al*, 1996].

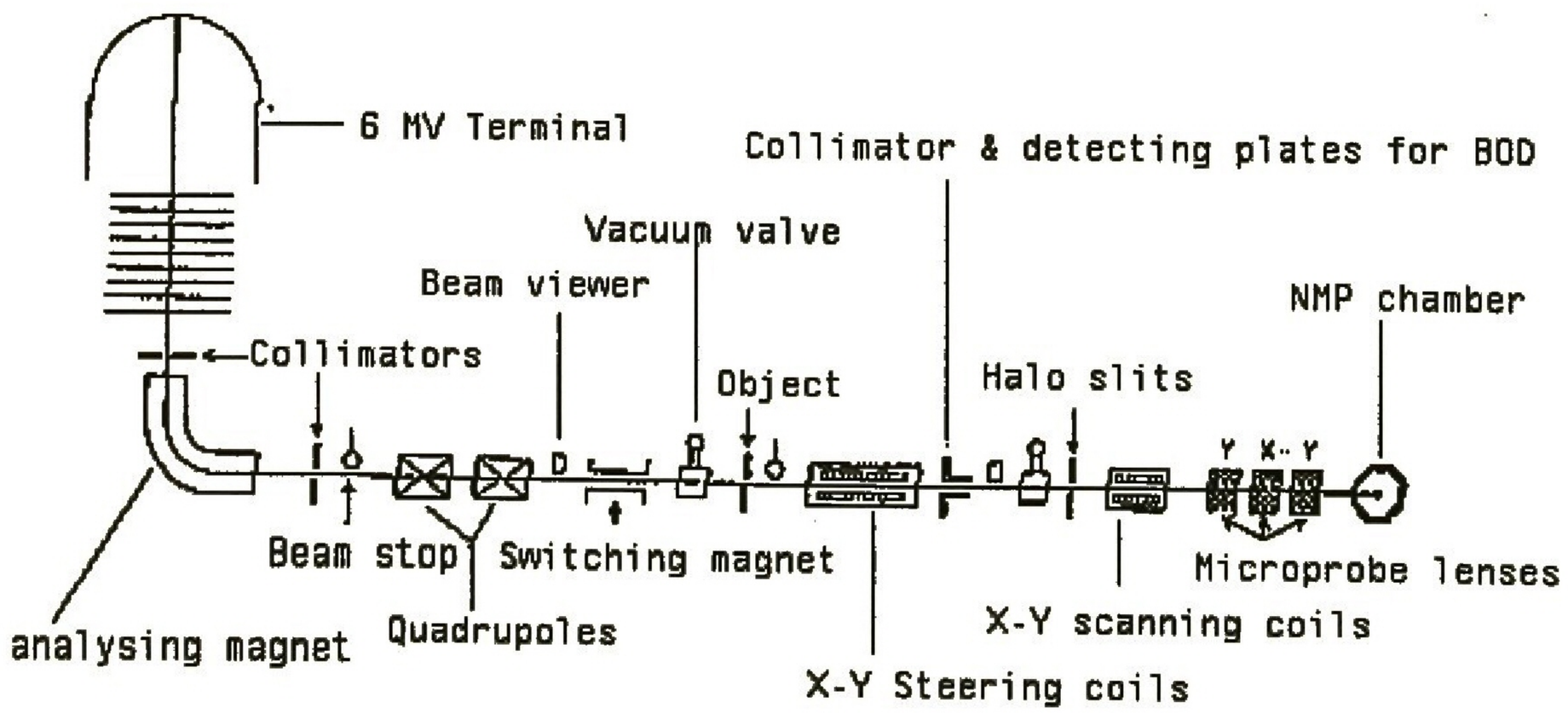

Figure .2.9. A schematic of the Van de Graff accelerator and NMP layout at iThemba LABS. Important features are shown. [Prozesky *et al*, 1995]

Chapter 3

3.1 Introduction

This chapter discusses the instrumentation and techniques employed in nuclear microprobe analysis. Methodology for data analysis is also described.

3.2 Standards

Pure metals mounted on the ladder were used as standards. Titanium nitride (TiN) layers deposited on steel by plasma vapour deposition were also used as standards in this study. This is because they have been accurately measured and the results have been published by Campbell and others (1994). Furthermore titanium nitride is now used as an example in GUPIX, so one can compare results not only with the publication but can also re-process the spectra from the publication. MicroMatter^{TM} standards$^{(*)}$ were also used for the study. Since these are standards therefore their values were known from the certified measurements done by the manufactures. PIXE and RBS were used to measure thickness and their results were compared. From the results, two methods showed good agreement for thickness.

(*) calibration standards for XRF analysis consisting of thin layers of metal evaporated on Mylar substrate

3.3 Thin metal layers on silicon substrate

Two sets of layers consisting of one pure element were deposited on Silicon wafer using the evaporator. One set had an additional layer of gold 100 nanometers (the layer

was deposited on silicon substrate and measured using 2 MeV alpha particles) thick between the metallic layer and silicon. The pure elements used were Magnesium, Aluminum, Titanium, Manganese, and Copper. The evaporator chamber consists of two areas. The top area has three crucibles onto which materials to be evaporated are loaded, an electron gun, a quartz thickness monitor and a sample changer. The quartz monitor determines the rate at which depositions are done as well as the thickness of the evaporated layers. The sample changer consists of six sample holders and each holder can mount eight samples. The bottom area consists of a Ti-sublimation pump and a cryopanel. During the cleaning of the crucibles and the loading of samples this part of the evaporator is kept under vacuum by closing the baffle valve. The turbo and rotary pumps are used to reduce the pressure at the top area to about 1×10^{-6} kPa. At this point the baffle pump is opened to allow the ion pumps to reach the vacuum of about 1×10^{-7} kPa. Liquid nitrogen is poured into the cryopanel for further improvement of the vacuum. The metals to be deposited are first preheated to release any absorbants before deposition is carried out. After deposition the samples are allowed to cool down before the evaporator is opened. After this whole process the samples together with the standards were washed with organic solvents. This was to remove any contamination of oxides. The solvents used in the sequence were methanol, acetone, trichloroethane, acetone and methanol. The methanol was then rinsed off or removed by washing the samples and standards with deionized water. The metals were dried and mounted on the sample holder in the nuclear microprobe.

3.4 Irradiation and measurement

The analysis was performed with 2.0 MeV alphas and 2.5 and 3.0 MeV protons, using the iThemba LABS nuclear microprobe. PIXE and RBS were simultaneously used. PIXE measurements were performed using two detectors for different sessions. A Si(Li) detector (manufactured by PGT [Princeton Gamma-Tech]) had the following parameters : 30 mm^2 active window, thickness of 3 mm with 8.5 µm Beryllium window. The resolution as measured by the manufacturer was 141 eV at 5.9 keV. High purity Germanium detector (manufactured by Eurisys) had the following parameters: 100 mm^2 active area, thickness of 7 mm with 12.5 µm Beryllium window. The resolution as measured by manufacturer was 145 eV at 5.9 keV. The detectors were positioned at 135^0 to the direction of the incoming beam. The backscattered protons were detected with an annular Silicon surface barrier detector positioned at 176^0. The beam current transmitted through a specimen was collected from a Faraday cup positioned behind the target. A copper ring situated in front of the target was used for secondary electron suppression with a negative voltage of -1500 volts. Proton beam current of about 1 nano-ampere was used in order to prevent possible damage to the samples during irradiation. The solid-state beam line chamber was also used for measurements using 2.0 MeV alpha particles for comparison with the nuclear microprobe.

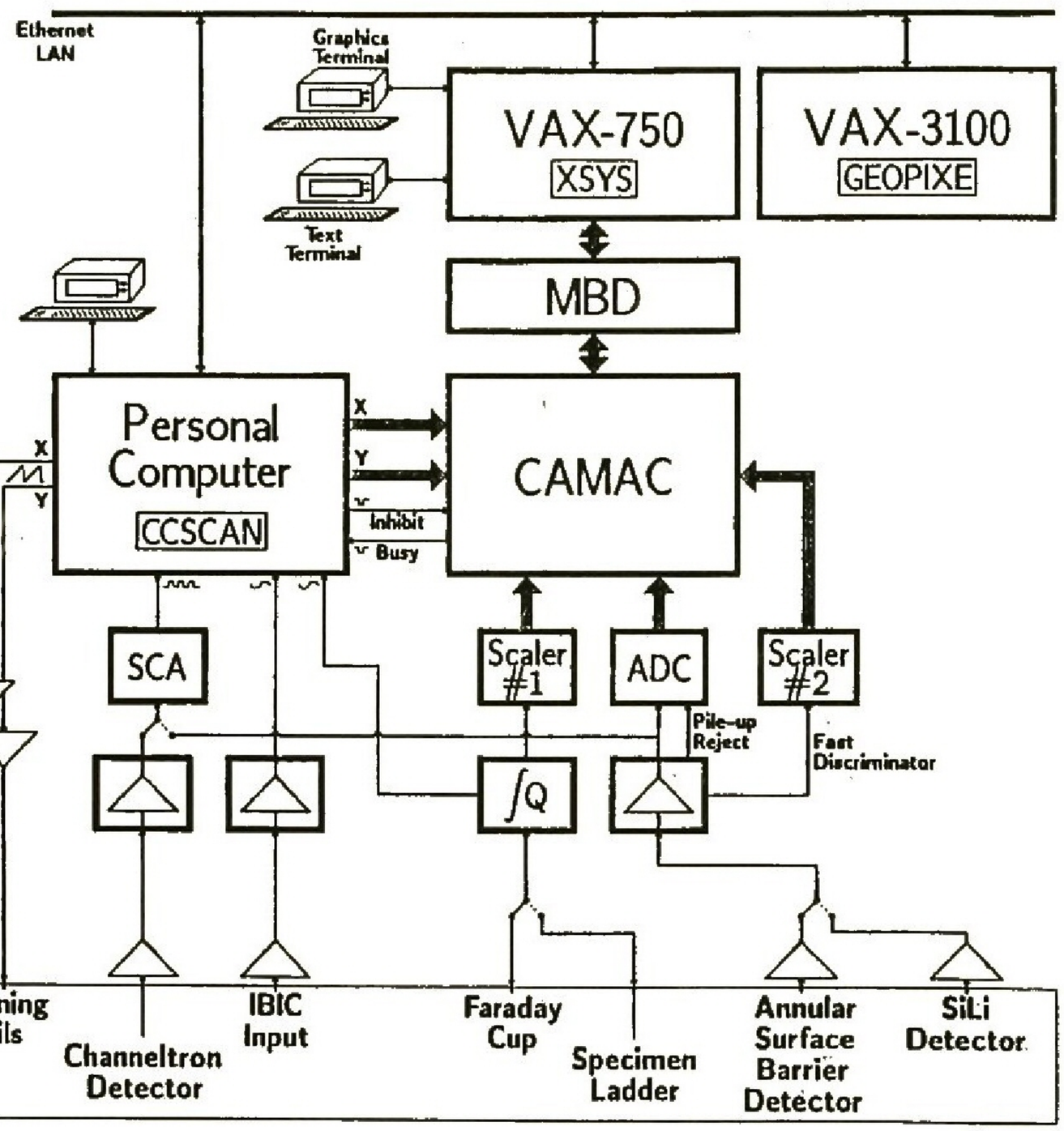

Figure 3.1. Schematic representation of data acquisition and control system of the iThemba LABS nuclear microprobe. [Churms et al 1993]

3.5 Data acquisition

The data acquisition system must be able to collect the signal from one or more detectors and store this signal with the corresponding spatial co-ordinate of the probe on the sample. The microprobe is interfaced to a CAMAC data acquisition system, fig. 3.1, which includes the data analysis software package XSYS. A 4000/VLC VAX station controls the acquisition and analysis of data. The XSYS general-purpose acquisition

system allows the use of complex arrays of data, with event-by-event storing capability, as well as the use of multi-parameter systems and multiple windows. A local PC interfaced to the steering coils controls the data acquisition, steering and positioning of the beam and the VAX using an in-house developed software package (Churms *et al*, 1993; Prozesky *et al*, 1995; Przybylowicz *et al*, 1999).

A further requirement of the data acquisition system is the need to display on-line spectra histograms and dynamic mapping images in real-time, (fig. 3.2.). This allows a researcher to monitor the quality of data and make some necessary adjustment to the actual measurement. The display system usually requires a separate computer from the one involved in the actual data collection.

3.6 Data processing

Spectra extracted from a data set that corresponds to regions of interest can be processed in many ways. There is a full range of conventional analysis techniques that can be applied to spectra acquired. For our study, RUMP, GUPIX and GeoPIXE are used.

RBS yields elemental and depth information. The analysis of RBS spectra is made easier with computer programs where the most useful programs are able to simulate spectra from given target information. RUMP software is mostly used for RBS and it includes all the calculations needed for the simulation module. The simulation module is used for theoretically constructing an RBS spectrum of a sample that consists of one or

more layers. When analyzing the actual data, the thickness of each layer is varied until the theoretical spectrum coincides with the actual data.

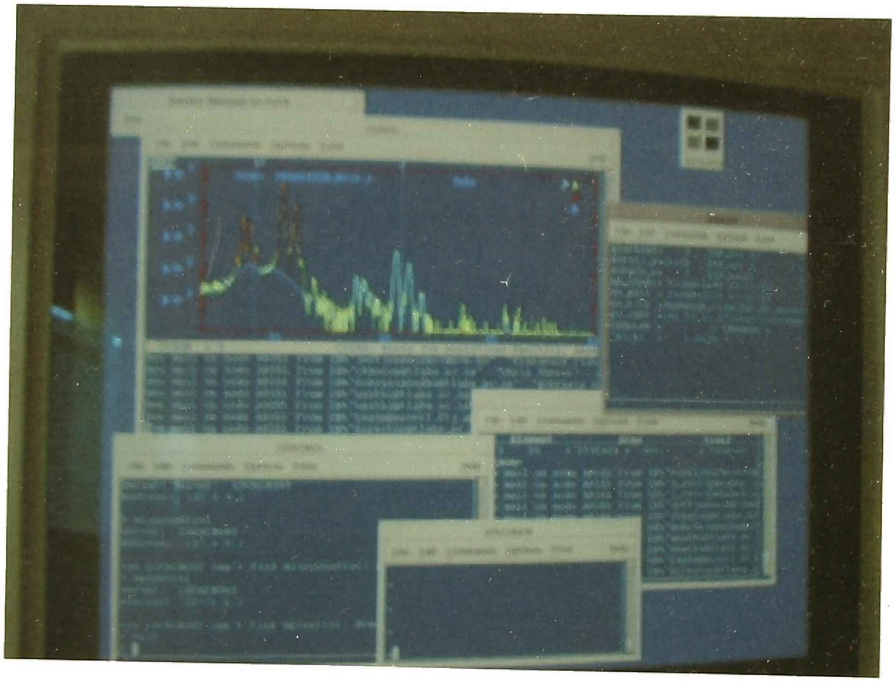

Figure 3.2. The data acquisition display system at the iThemba LABS showing windows with selected regions of interest and the corresponding energy spectra.

RBS yields elemental and depth information. The analysis of RBS spectra is made easier with computer programs where the most useful programs are able to simulate spectra from given target information. RUMP software is mostly used for RBS and it includes all the calculations needed for the simulation module. The simulation module is

used for theoretically constructing an RBS spectrum of a sample that consists of one or more layers. When analyzing the actual data, the thickness of each layer is varied until the theoretical spectrum coincides with the actual data.

In PIXE, depth information, composition and concentration can be extracted by using information contained in the spectra with the aid of the software packages GUPIX and GeoPIXE. GUPIX allows for iterative thickness determination when the specimen thickness is unknown. PIXE spectra are fitted and the resulting peak intensities are converted to areal densities. The areal densities are summed to provide an initial estimate of the specimen thickness. GeoPIXE offers mostly concentration yield and elemental identification and it can detect all these at very low concentrations. Detection sensitivities as low as 0.2 ppm can be achieved. Although GeoPIXE can fit spectra of complex multi-layered specimen, it does not have a subroutine for automatic iterative calculation of the layer thickness.

Chapter 4

Measurements have been performed using

- Two techniques: RBS and PIXE
- Various types of particles and energies (2 MeV alpha particles, 2.5 MeV and 3 MeV protons)
- Different measurement chambers (nuclear microprobe and solid-state chambers, at two separate beam lines)
- Some PIXE measurements were performed using two detectors, Si(Li) detector (PGT) and a high purity Ge detector (Eurisys)

The 2 MeV alpha particles were used because they are the most often used type of particle and energy in the characterization of thin layers when using RBS. The cross sections at this energy are well known and the assumption that the backscattering process is described by elastic-Rutherford scattering is valid. Therefore one can expect reliable RBS measurements at this energy.

Protons were used because most PIXE measurements are performed with protons and the most often used energy at iThemba LABS is 3 MeV. At these energy PIXE parameters, cross-sections in particular, are well characterized and can be used with confidence. Use of proton backscattering at this energy also presents advantages because cross-sections for some elements, light ones in particular, show resonances. Although this present some difficulties because the cross-sections are not always accurately known, the sensitivity of BS technique can sometimes be better in

comparison with routine analysis with 2 MeV alpha beam. The beam penetrates a specimen much deeper and this presents benefits for thickness evaluation.

The use of 2.5 MeV protons was mostly dictated by the fact that iThemba LABS does not have reliable cross-sections for nitrogen measurements in the energy range between 2.5 MeV and 3 MeV, at the required angle (176 degrees). Therefore the recently published nitrogen cross-sections up to 2.5 MeV have been used (Ramos *et al.* 2002).

Measurements using two experimental chambers were performed in order to compare two methods of charge collection. The chamber used exclusively for BS work (Solid-state chamber) is evacuated from the rest of the beam line. This method of charge collection is different from the one used in the nuclear microprobe, where charge is collected from the ladder on which the specimens are mounted. In cases where beam penetrates through the specimen, beam charge is collected simultaneously from the ladder and the Faraday cup positioned behind a specimen. The charge collection is improved by using electron suppressor in front of a specimen.

In earlier measurements related to thin layer characterization, the results were obtained as relative, e.g. normalized to the substrate signal (often silicon substrate), and not much attention was paid to the absolute charge collection. Comparison between results performed at two chambers, on well-characterized specimens, can serve as a good test of charge collection in both cases.

4.1. Backscattering measurements

Energy calibration was done using RUMP related package GENPLOT and the simulations were done based on the energy calibration parameters. In energy calibration the channel versus energy of each pure element is plotted and this energy calibration is used for all other spectra collected at a specific type of beam and energy.

4.1.1. Comparison of results from two experimental chambers (NMP and SS) using 2.0 MeV alpha particles.

Energy calibration was made using a set of three standards consisting of pure elements - silicon, titanium and iridium for the solid-state line and zirconium was added for the nuclear microprobe chamber. The energy calibration was considered to be acceptable when the simulations with RUMP fitted the experimental spectra, figure 4.1. b-d and h-k. The samples of titanium nitride deposited on steel substrate were measured in both chambers and they all showed good agreement except for the little mismatches at high and low energies. The mismatches at low energies were due to multiple scattering whereas at high energies were due to pile-ups resulting from high-count rates. In addition the absence of the pile-up rejection system in the nuclear microprobe may have also contributed [*]. The iron peak was observed near channel 100 (figure 4.1.(l)). The presence of this peak means that the beam penetrated through the TiN layer and reached the steel substrate. It was speculated that there might be a tantalum contamination that might have resulted from its prior use in the deposition system. As

speculated, it was found that tantalum was present and a small tantalum peak was noticed at the tail of all the TiN spectra.

It was also observed that there was some inconsistency in the values of correction factors in simulations of standards when using alpha particles (table 4.1.). The correction factor values were found to be increasing as the atomic number of an element increases. This phenomenon is consistent with earlier measurements performed using alpha particles in the nuclear microprobe chamber (Ryan and van Achterbergh, 1993). An error in the integrated charge measurement was attributed to the loss of the electron in the H_2^+ molecule scattered from the sample surface. Owing to the center-of-mass motion of the H_2^+ molecule, even the relatively low velocity distribution of the bound electron results in a velocity distribution for the electron in the laboratory frame extending beyond 1.5 keV. Evidently, many of these electrons are not trapped by the suppressor arrangement. The registration of false (incomplete) charge requires changes of the correction factor during simulations. It is interesting to note that the same problem with incomplete charge collection was observed in the solid-state chamber (Table 4.1.), although the effect was smaller than in the nuclear microprobe chamber. There were no earlier reports on the incomplete charge collection in the evacuated solid-state chamber. The correction factors for the TiN specimen were almost constant. This was due to that the matrix composition was the same throughout. What can be also observed is that the alpha particles have low sensitivity for light elements since the weak N signal is submerged in the background produced by Ti atoms. However the overall simulations for 2 MeV alpha particles in both the solid state and nuclear microprobe chamber showed good agreement .

(*) the first set of BS spectra from the measurements in the nuclear microprobe was obtained without the pile-up rejection system

Table 4.1. Comparison of correction factors between the NMP and SS chambers.

Solid-state chamber	
Silicon	1.02
Titanium	1.20
Iridium	1.90
Sample D-1	0.90
Sample D-4	0.98
Sample D-6	0.98
Nuclear microprobe chamber	
Silicon	1.25
Titanium	1.32
Zirconium	1.87
Iridium	2.58
Sample D-1	1.19
Sample D-4	1.28
Sample D-6	1.25

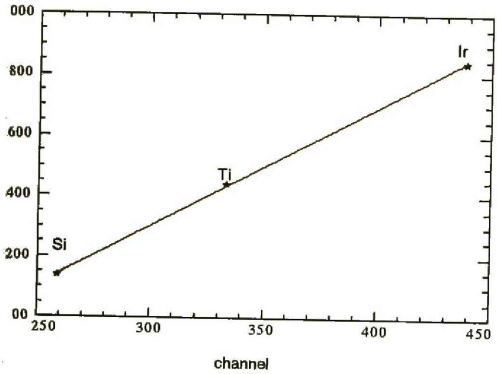

Figure 4.1.(a) Energy vs channel calibration curve from GENPLOT for 2.0 MeV alpha particles.

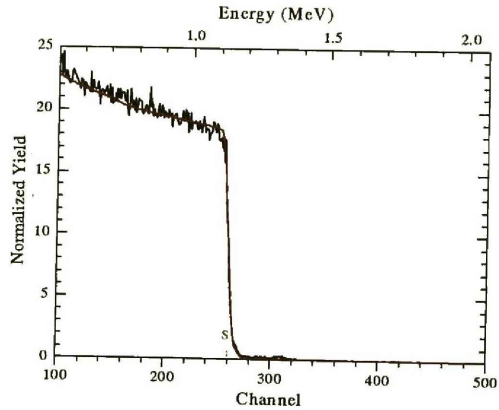

Figure 4.1.(b) Experimental spectrum (Black) and simulation (Red) of Silicon for 2.0 MeV alpha particles in the SS chamber.

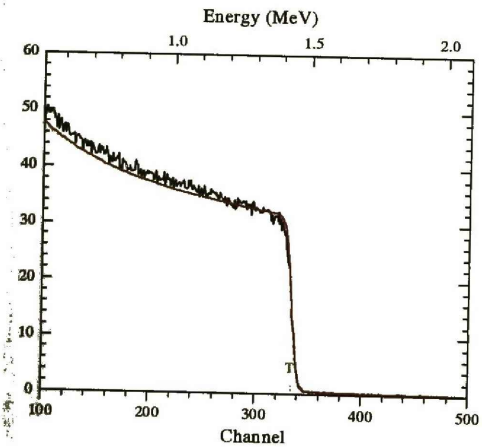

Figure 4.1.(c) Experimental spectrum (Black) and simulation (Red) of Titanium for 2.0 MeV alpha particles in the SS chamber .

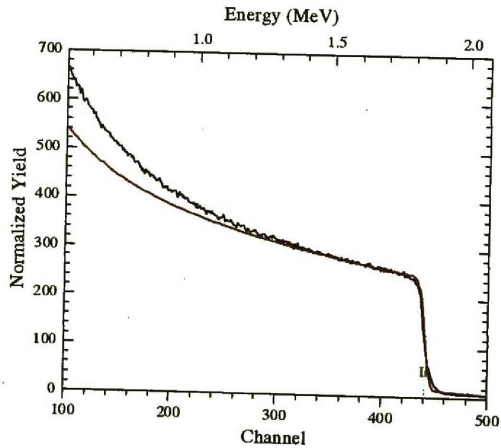

Figure 4.1.(d) Experimental spectrum (Black) and simulation (Red) of Iridium for 2.0 MeV alpha particles in the SS chamber .

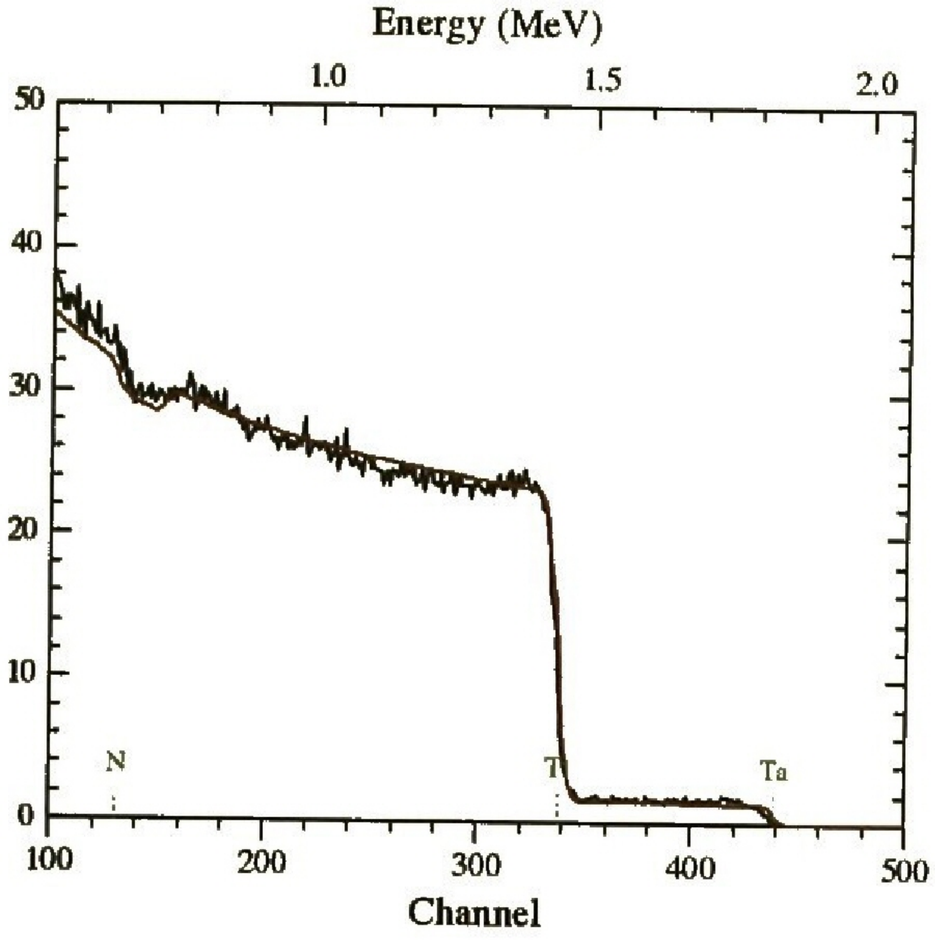

Figure 4.1.(e) Experimental spectrum (Black) and simulation (Red) of TiN on steel (Sample D-1) for 2.0 MeV alpha particles in the SS chamber

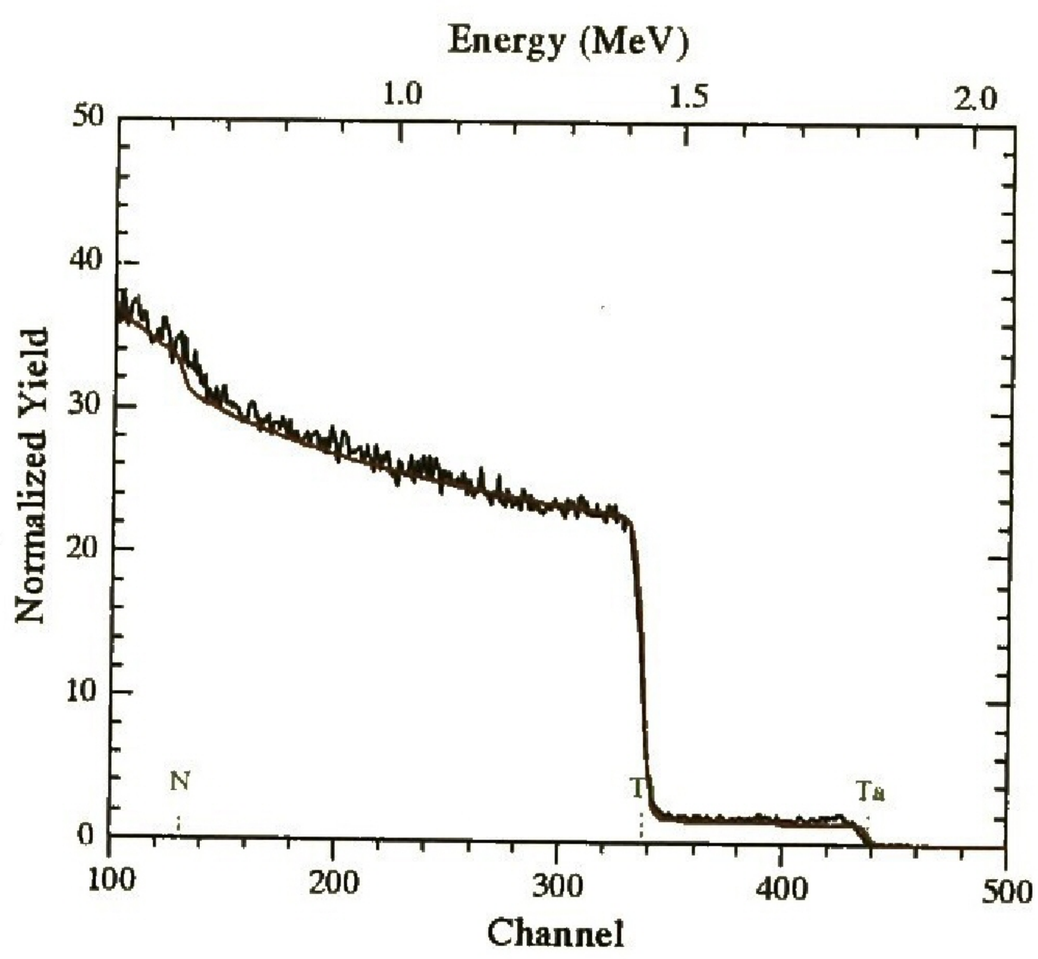

Figure 4.1.(f) Experimental spectrum (Black) and simulation (Red) of TiN on steel (Sample D-4) for 2.0 MeV alpha particles in the SS chamber

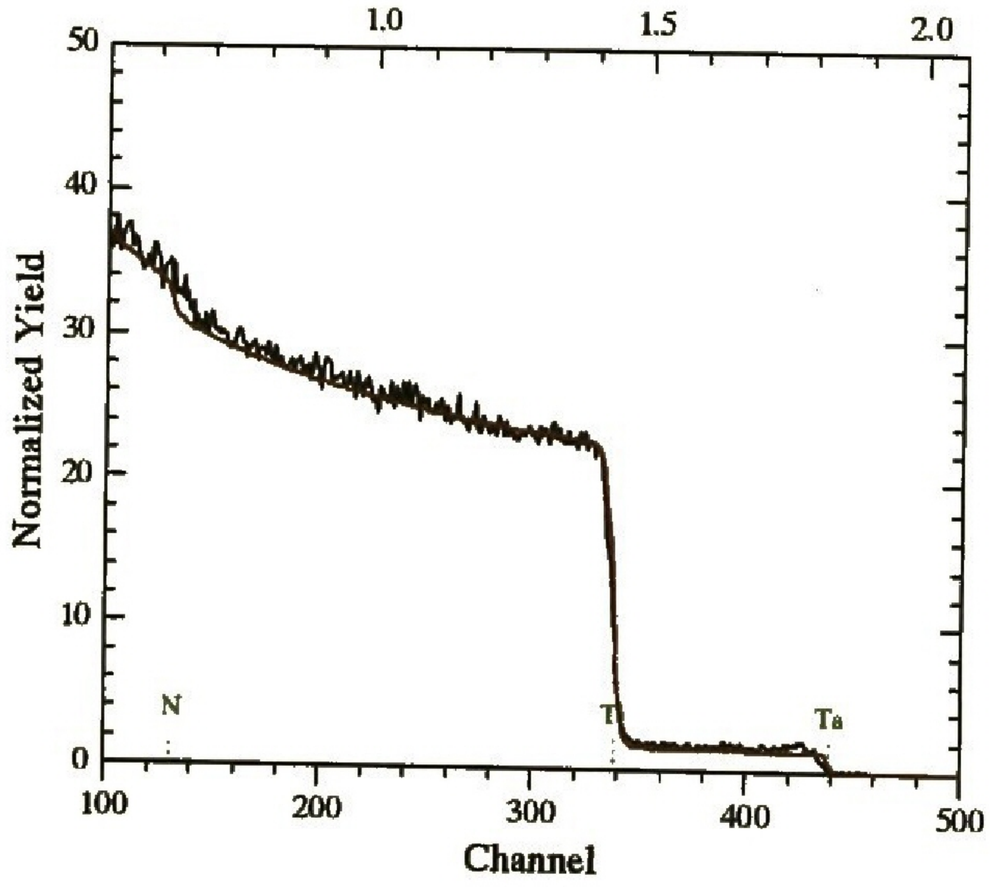

Figure 4.1.(g) Experimental spectrum (Black) and simulation (Red) of TiN on steel (Sample D-6) for 2.0 MeV alpha particles in the SS chamber

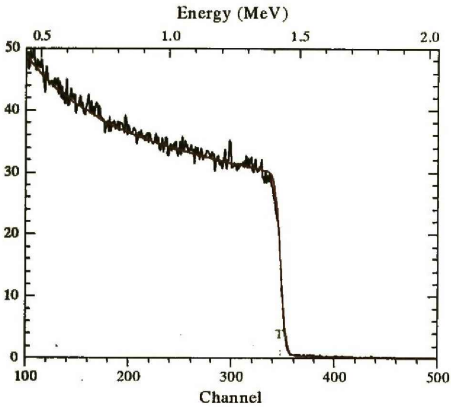

Figure 4.1.(h) Experimental spectrum (Black) and simulation (Red) of Titanium for 2.0 MeV alpha particles in the NMP chamber.

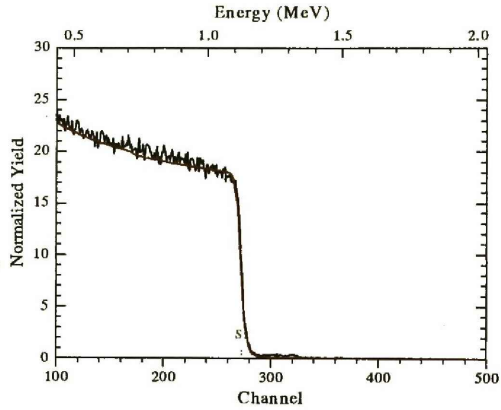

Figure 4.1.(i) Experimental spectrum (Black) and simulation (Red) of Silicon for 2.0 MeV alpha particles in the NMP chamber.

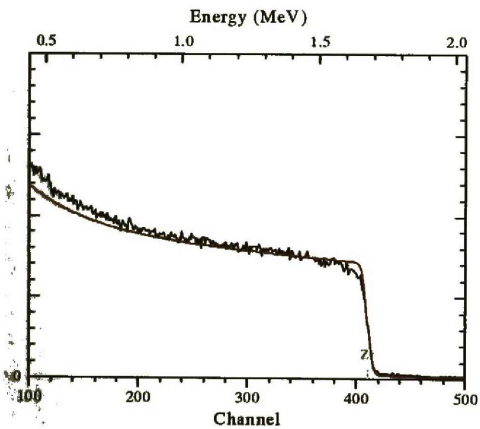

Figure 4.1.(j) Experimental spectrum (Black) and simulation (Red) of Zirconium for 2.0 MeV alpha particles in the NMP chamber .

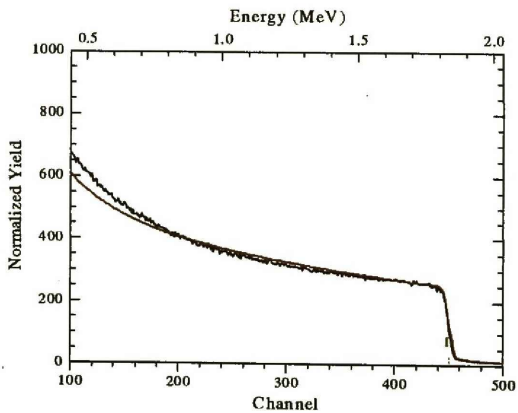

Figure 4.1.(k) Experimental spectrum (Black) and simulation (Red) of Iridium for 2.0 MeV alpha particles in the NMP chamber.

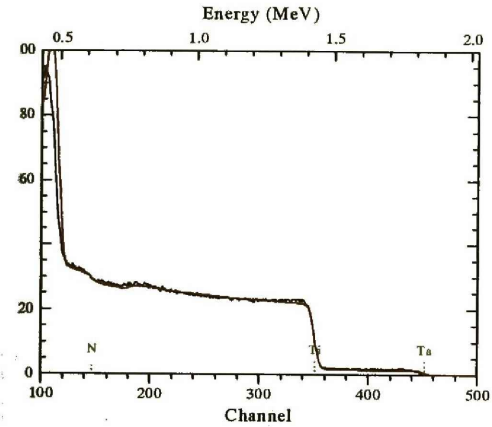

igure 4.1.(l) Experimental spectrum (Black) and simulation (Red) of TiN steel (Sample D-1) for 2.0 MeV alpha particles in the NMP chamber

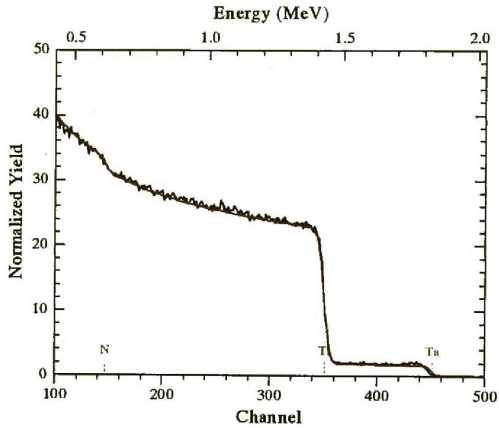

Figure 4.1.(m) Experimental spectrum (Black) and simulation (Red) of TiN on steel (Sample D-4) for 2.0 MeV alpha particles in the NMP chamber

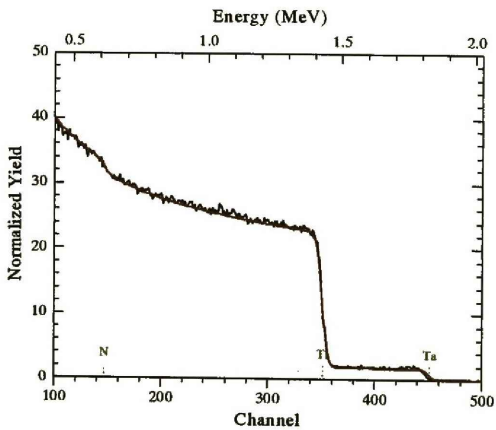

Figure 4.1.(n) Experimental spectrum (Black) and simulation (Red) of TiN on steel (Sample D-6) for 2.0 MeV alpha particles in the NMP chamber

4.1.2. Comparison of RUMP and GUPIX using both chambers.

Backscattering spectrometry by itself is generally used for obtaining depth distribution and elemental concentration in the sample layers especially the surface ones. This information was used to evaluate layer thickness and elemental concentration of titanium nitride layer on a steel substrate. The evaluated samples were of different thickness.

PIXE spectra were evaluated using GUPIX software (Campbell *et al*, 2000). GUPIX evaluation includes matrix elemental concentration determination and layer thickness measurement. For thickness determination using GUPIX, the two approaches are used. In the first approach the exit proton energy from a layer is varied until the total concentration of the matrix elements in that layer converges to one. For the second approach the exit proton energy of the layer is varied until the total concentration of the matrix elements of the substrate converges to one. The thickness iteration option is chosen and the program determines the layer thickness. The program has also an option where one can specify whether the layer is thick or thin. These options are usually used if the layers to be measured are too thin and also when option two of PIXE cannot be used.

Table 4.2. Results of RBS and PIXE measurements from the publication, solid-state chamber and the nuclear microprobe chamber.

Measurements from Publication					
Sample	Relative composition (atomic fraction)			Thickness [mg/cm^2]	
	Ti	N	Ta	RBS	PIXE
D1	0.495	0.502	0.003	0.51	0.55
D4	0.524	0.472	0.004	1.44	1.42
D6	0.515	0.482	0.003	2.35	2.36
RBS measurements from SS chamber for 2 MeV alpha particles					
Sample	Relative composition (atomic fraction)			Thickness [mg/cm^2]	
	Ti	N	Ta		
D1	0.518	0.479	0.003	0.484	
D4	0.495	0.502	0.003	≥ 0.684	
D6	0.495	0.502	0.003	≥ 0.684	
BS measurements from NMP chamber for 2 MeV alpha particles					
Sample	Relative composition (atomic fraction)			Thickness [mg/cm^2]	
	Ti	N	Ta		
D1	0.495	0.502	0.003	0.484	
D4	0.524	0.472	0.004	≥ 0.684	
D6	0.500	0.496	0.004	≥ 0.684	
PIXE measurements from NMP chamber for 2 MeV alpha particles					
Sample	Relative composition (atomic fraction)			Thickness [mg/cm^2]	
	Ti	N	Ta	PIXE [1]	PIXE [2]
D1	0.499	0.498	0.003	0.550	0.550
D4	0.498	0.498	0.004	≥ 0.550	
D6	0.498	0.498	0.004	≥ 0.550	

Table 4.2 shows both the elemental concentration and layer thickness of the samples. It was noticed that the concentrations of all elements were more or less constant and the contamination with low tantalum concentration was confirmed. However the elemental composition for PIXE measurements was found to be almost constant. In both techniques the correct layer thickness was found only for sample D1. These results were considered to be acceptable for both techniques since they matched the published values, which are 0.51 and 0.55 mg/cm^2 for RBS and PIXE respectively. The values were considered accurate because when compared to the published results the statistical error was found to be about 5% for RBS and 1% for PIXE. Layer thicknesses for samples D4 and D6 could not be determined at this energy as they were too thick for the energy used. The simulations have confirmed this with varied TiN thickness, which proved that the layer thickness can be evaluated only up to 0.684 mg/cm^2. Since option two is dependent on the X-rays from the substrate, there were no results for PIXE and this was due to that the particle energy could not reach the substrate layer therefore no X-rays were produced to give some yield which allows one to compute layer thickness. The results also confirmed that PIXE is a reliable method for measuring thickness since when compared with RBS the results showed good agreement. It was therefore concluded that high-energy beams were essential for thickness measurements especially for samples D4 and D6 and when thicker samples are to be measured in both the solid-state and the nuclear microprobe chambers. The overall conclusion from these results was that for thickness to be determined for samples D4 and D6, alpha particles of higher energies must be used.

In order to have correct thickness measurements in PIXE, the H-value has to be correctly determined. The following tables show the results obtained from both the publication and the experiments. Table 4.3. shows the results of H values from the three standards.

Table 4.3. Results of H values from standards of pure elements for 2 MeV alpha particles and 2.5 MeV protons in the NMP chamber.

Element	H value	
	2 MeV alpha particles	2.5 MeV protons
Titanium	1.81E-02	3.56E-02
Zirconium	3.80E-02	3.04E-02
Iridium	3.52E-02	3.40E-02

Table 4.3 shows H-values as obtained from the pure standards. The value for titanium at 2 MeV is different from the rest. This is due to the difference in filter absorption. At this energy the X-rays are of low energy hence they are absorbed by the filter. The value of 3.4×10^{-2} was used for the experiment. The value is the mean of the H-values, which were closer to one another. This H-value was used for both 2 MeV alpha particles and 2.5 MeV protons energies since the experimental geometry was the same.

4.1.3. Elemental concentration using GeoPIXE

GeoPIXE has been developed for more specific application and it offers mostly concentration yield and elemental identification and it can detect all these at very low

concentrations. The following table shows the elemental concentration in percentage for the TiN samples for 2.0 MeV alpha particles.

Table 4.4. Results of elemental concentration measurements from GeoPIXE.

Element	Concentration (%) (mass)	
Titanium	34	
Zirconium	103	
Iridium	148	
	Ti	Ta
D-1	48	2.42
D-4	36.7	2.17
D-6	37.5	2.38

The concentration for pure elements showed discrepancies. Their concentrations were expected to be close to 100% and this was not the case. The same problem occurred in the TiN samples. As the program cannot find the layer thickness iteratively, the only possibility to obtain the results is to enter the thickness layer found elsewhere (from GUPIX or from the reference publication) and to compare the obtained elemental concentration (in this case Ti and Ta) with the earlier results. The elemental concentration for titanium was found to be low as compared to the publication. The conclusion based on the above results was that GeoPIXE software could not be trusted for elemental concentration in this particular study.

4.2. Results of TiN from NMP using 2.5 MeV protons.

Simulations of TiN were also done using 2.5 MeV protons. Simulation process at this particular energy is dependent on the availability of cross sections. This is due to that at higher energies (> 2.4 MeV) (Vizkelethy, 1994) the elastic cross sections start to deviate from Rutherford. Therefore the non-Rutherford cross-sections improve the detection of light elements on heavier substrate (Amirikas *et al*, 1993). Hence one was able to clearly observe the nitrogen peaks that were not clear with energies of 2.0 MeV alpha particles. It was also observed that the use of 2.5 MeV protons result in simulations of thicker samples corresponding well with the experimental data. The simulations were considered to be good since they came out as expected.

Thickness determination was also done on the titanium nitride (TiN) on steel substrate samples at 2.5 MeV protons. Table 4.5 shows the calculated thickness and the elemental concentrations of each sample from RUMP and GUPIX at 2.5 MeV protons. Elemental concentration remained almost constant for each element in both techniques and the low tantalum concentrations were due to the fact that it was a contaminant therefore it was expected at very low concentration values. The layer thickness of the samples was calculated in both techniques and the recorded results showed good agreement when compared with each other. The results were then compared with the results published earlier (table 4.5).

Table 4.5. Results of RBS and PIXE measurements from the publication and the nuclear microprobe chamber.

Measurements from Publication					
Sample	Relative composition (atomic fraction)			Thickness [mg/cm^2]	
	Ti	N	Ta	RBS	PIXE
D1	0.495	0.502	0.003	0.51	0.55
D4	0.524	0.472	0.004	1.44	1.42
D6	0.515	0.482	0.003	2.35	2.36
RBS measurements using RUMP for 2.5 MeV protons					
Sample	Relative composition (atomic fraction)			Thickness [mg/cm^2]	
	Ti	N	Ta		
D1	0.502	0.495	0.003	0.515	
D4	0.511	0.485	0.004	1.449	
D6	0.505	0.491	0.004	2.388	
PIXE measurements using GUPIX for 2.5 MeV protons					
Sample	Relative composition (atomic fraction)			Thickness [mg/cm^2]	
	Ti	N	Ta	PIXE [1]	PIXE [2]
D1	0.499	0.498	0.003	0.578	0.531
D4	0.498	0.498	0.004	1.523	1.401
D6	0.498	0.498	0.004	2.399	2.637

From the comparison with earlier published results it was observed that the two methods showed acceptable agreement because the statistical error was between 0.6% and 1.6% for RBS and 1.6% and 11% for PIXE. Based on the comparison of results it was observed that PIXE could be used to measure surface layer thickness. From these results it was concluded that PIXE has the ability to measure thickness independently and to confirm this, own samples were prepared and their thickness evaluated.

4.2.1. Elemental concentration using GeoPIXE

Table 4.6. Results of elemental concentration measurements from GeoPIXE.

Element	Concentration (%) (mass)	
Titanium	99.7	
Zirconium	88.7	
Iridium	94.8	
	Ti	**Ta**
D-1	70	1.5
D-4	64	1.8
D-6	65	1.6

The elemental concentration for pure elements was considered acceptable since they were found to be around 100%. The TiN samples elemental concentration also showed discrepancies when compared with the published GUPIX results. The concentrations were expected to be around 75% for titanium. Iron here is not shown since it is a substrate. The conclusion was that these results were considered valid because the agreement between experimental and published results was between 86% and 92% hence GeoPIXE could be trusted for these results.

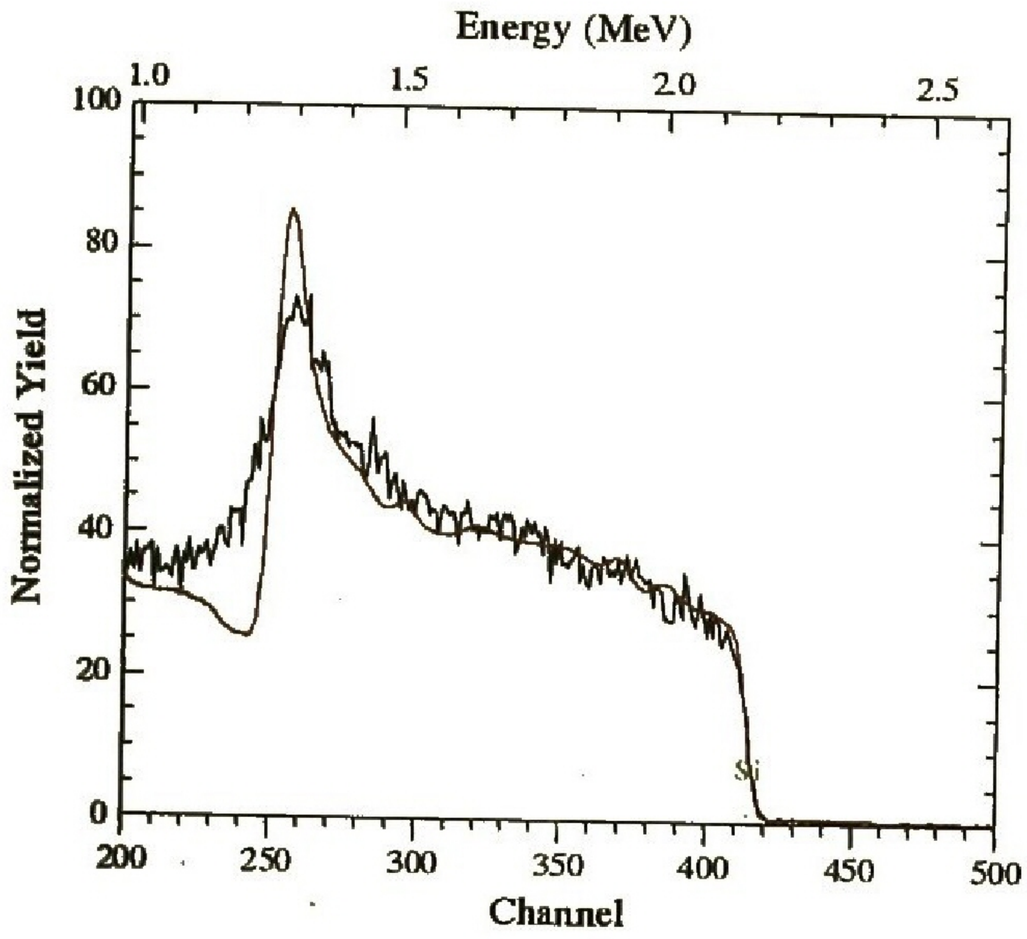

Figure 4.2.(a) Experimental spectrum (Black) and simulation (Red) of Silicon for 2.5 MeV protons in the NMP chamber.

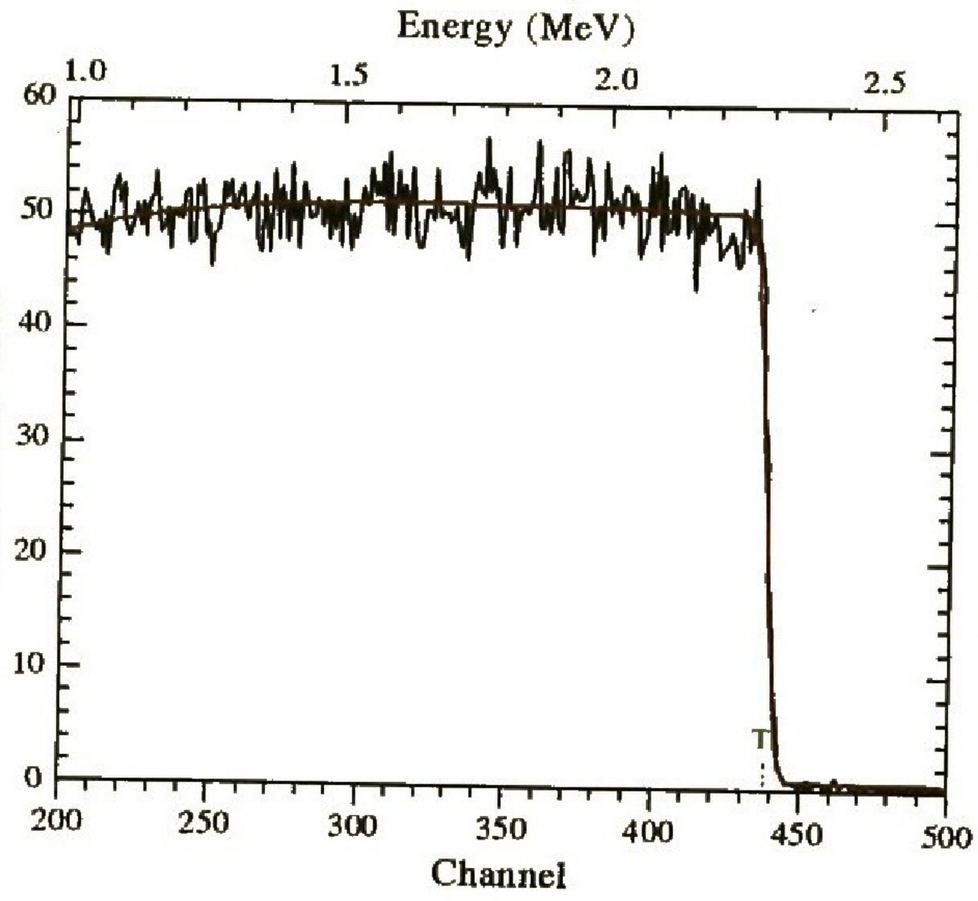

Figure 4.2.(b) Experimental spectrum (Black) and simulation (Red) of Titanium for 2.5 MeV protons in the NMP chamber.

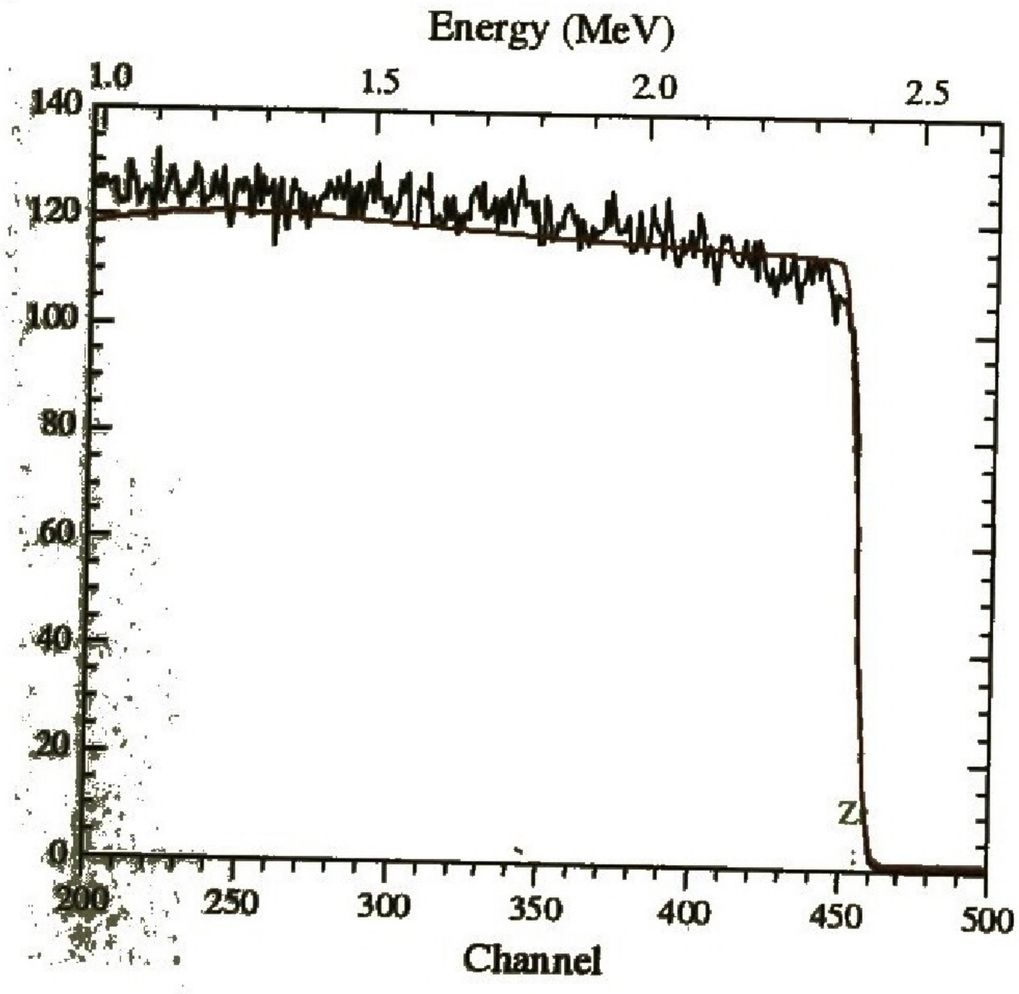

c) Experimental spectrum (Black) and simulation (Red) of
or 2.5 MeV protons in the NMP chamber.

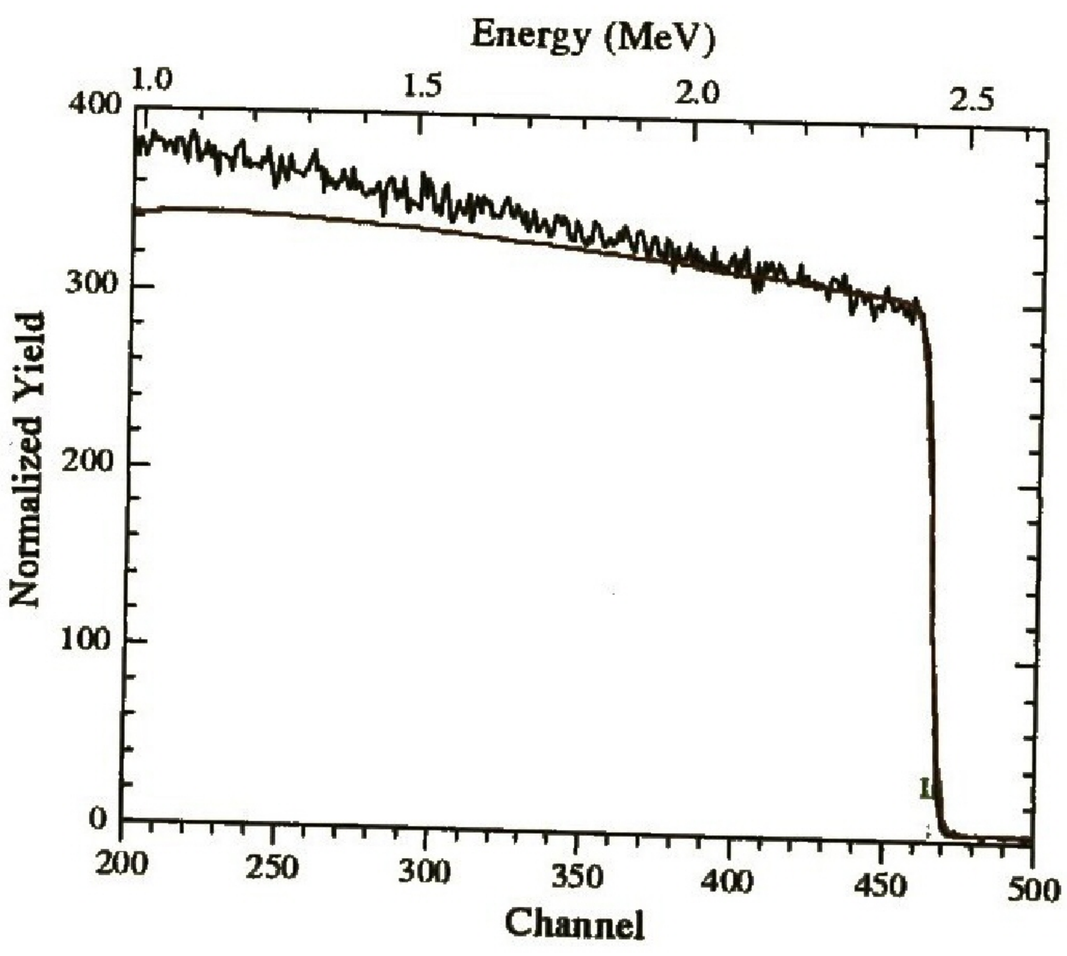

Figure 4.2.(d) Experimental spectrum (Black) and simulation (Red) of Iridium for 2.5 MeV protons in the NMP chamber.

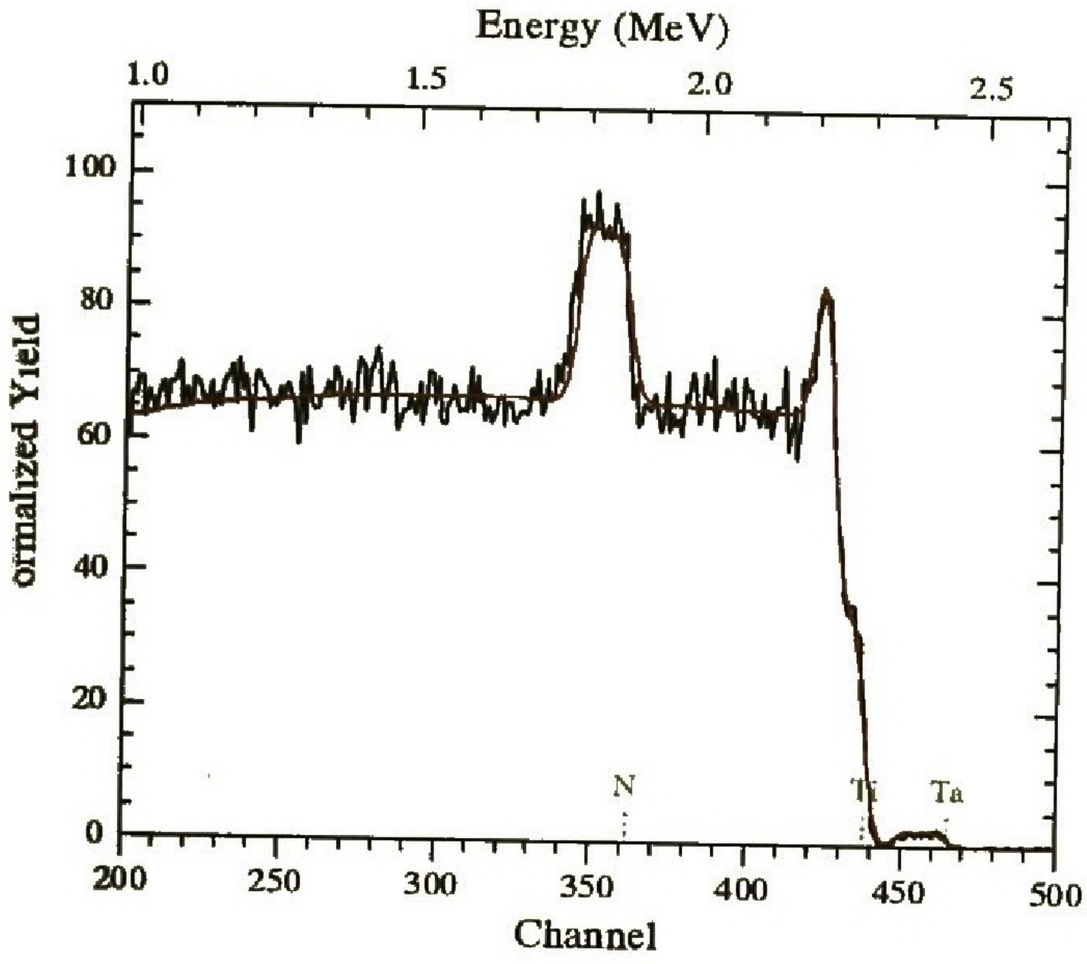

Figure 4.2.(e) Experimental spectrum (Black) and simulation (Red) of TiN on steel (Sample D-1) for 2.5 MeV protons in the NMP chamber

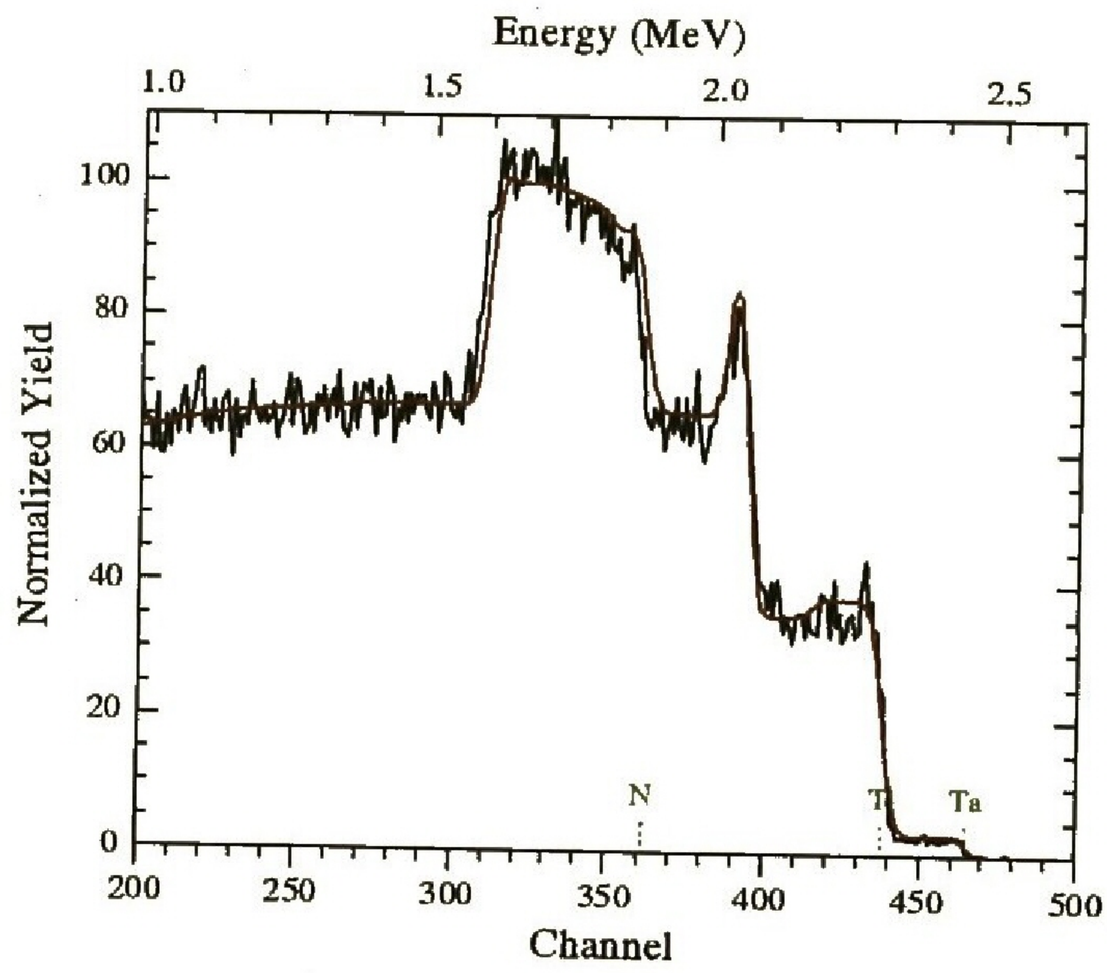

Figure 4.2.(f) Experimental spectrum (Black) and simulation (Red) of TiN on steel (Sample D-4) for 2.5 MeV protons in the NMP chamber

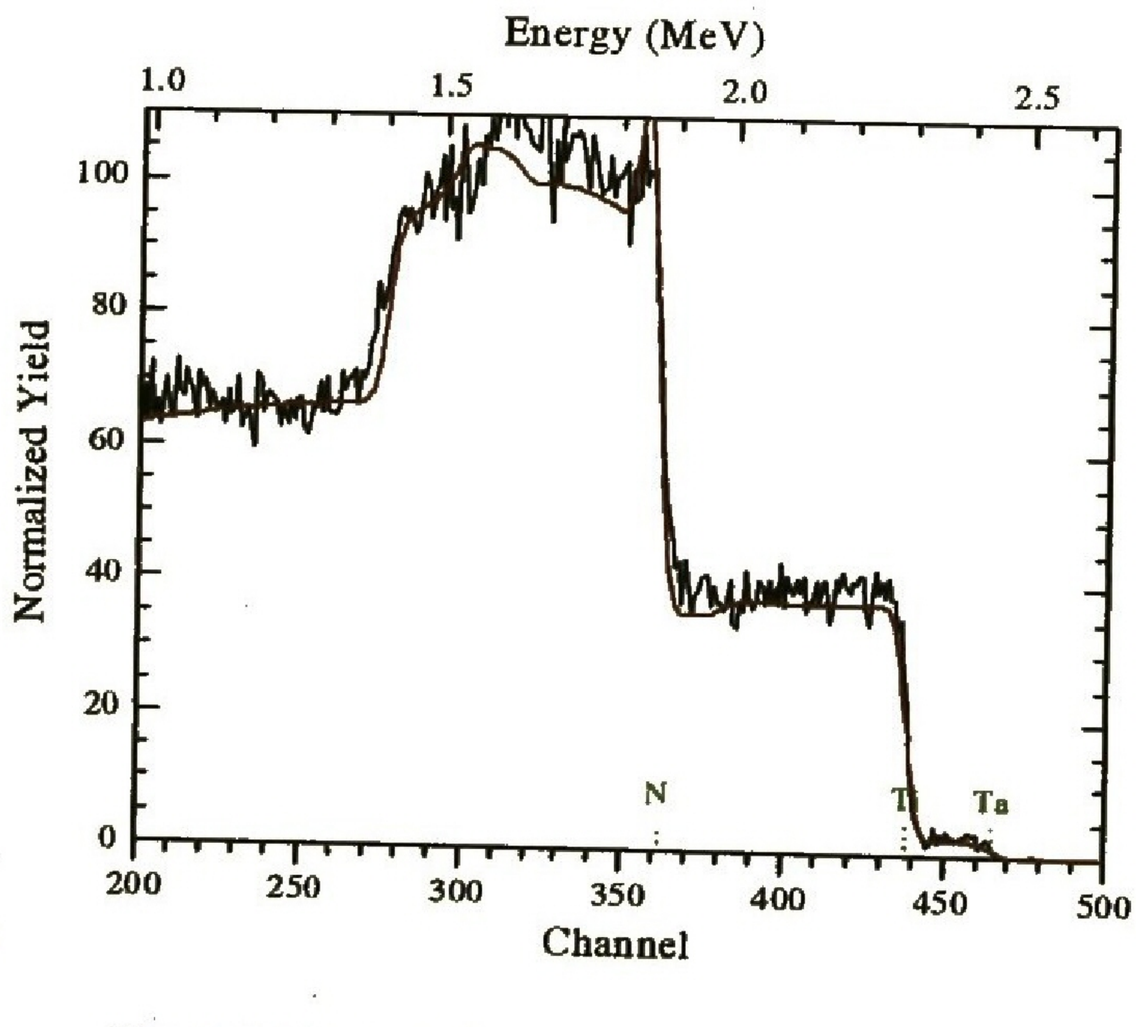

Figure 4.2.(g) Experimental spectrum (Black) and simulation (Red) of TiN on steel (Sample D-6) for 2.5 MeV protons in the NMP chamber

4.3. Results of MicroMatter™ standards from NMP using 3 MeV protons.

Simulations and thickness measurements were again done on the MicroMatter™ standards. The energy used for this study was 3.0 MeV protons and a high purity Germanium X-ray detector was used. The beam on-demand deflection system was not used because it was faulty at the time of analysis. The MicroMatter™ standards thickness measurements were then compared with the certified values in order to confirm the ability of PIXE in thickness evaluation. The measured spectra and RUMP simulations are shown in figure 4.3 (a-g). The simulations showed good agreement. The correction factor was also constant in all cases.

Thickness measurements were done for BS and the values were compared to the certified ones. For PIXE, the system H value was determined using six standards. The table below shows the measured H values from the standards

Table 4.7. H values as measured from pure standards were obtained using K X-ray lines except for Au, obtained using L X-ray lines.

Element	H value
Fe	0.106
	0.101
	0.099
	0.095
	0.097
(L)	0.086

The H value should remain constant for the K X-rays for elements in the range $20 \leq Z \leq 50$. The H value used was the mean of results for five elements (Fe - Ag) measured using K X-rays lines. Gold was not used due to discrepancies from L line X-rays(*). The mean value was found to be 0.0996. This value was used for thickness measurements in GUPIX for MicroMatter™ standards, thin metals on silicon and thin metals on gold on silicon substrate. The table below shows comparison of BS and PIXE results with the certified values.

Table 4.8. Comparison of certified values for MicroMatter™ standards with the measured ones from RBS and PIXE for 3.0 MeV protons in the nuclear microprobe chamber.

Sample	Thickness [μg/cm²]			
	Certified	BS	Thin layer	Thick layer
Al	44.7	76	53.56	4.01
Ti	40.6	36.0	25.87	25.94
Cr	42.7	47.5	32.24	32.78
Fe	49.9	49.16	38.56	38.66
Zn	49.5	45.6	40.09	40.18
Ag	48.2	46.5	43.40	43.4
Sn	46.2	44.3	44.97	45.03

(*) Due to some inaccuracies in the database for L X-ray lines it is preferable to measure H-value separately for K and L groups of X-ray lines rather than using the same H-value for both groups.

The MicroMatter™ samples were thin and that meant that the accelerated particles lose only a small part of their energy when passing through them. This meant that the excitation energy was well defined and that there was little absorption of the emitted X-rays in the specimen, which simplified the X-ray yield calculations. The results showed good agreement except for aluminum, which showed different results. For backscattering, the high value was due to that the counts of the substrate (mylar in this case) are incorporated with the ones for the surface element. For PIXE the reason was that the beryllium filter absorbs 98 % of aluminum X-ray at this energy range. Therefore aluminum cannot be detected. Titanium also showed different results. For BS the low values may be attributed to incorrect cross sections. For PIXE the cause is not known since all the parameters were considered to be correct. However, these discrepancies of PIXE results might be related to the lack of beam on-demand deflection system. In such case charge for PIXE can be over-estimated (because during time intervals for processing PIXE pulses the charge is still counted) and this would lead to under-estimation of concentrations. However when compared with the certified values, the BS results showed good agreement since the systematic error was found to be less than 10%. PIXE results showed some slight differences. The systematic error for PIXE when compared with the certified values was found to be between 10 and 36%. These results were considered not satisfactory. Therefore based on the systematic error it was concluded that BS could determine layer thickness better than PIXE does for these studies.

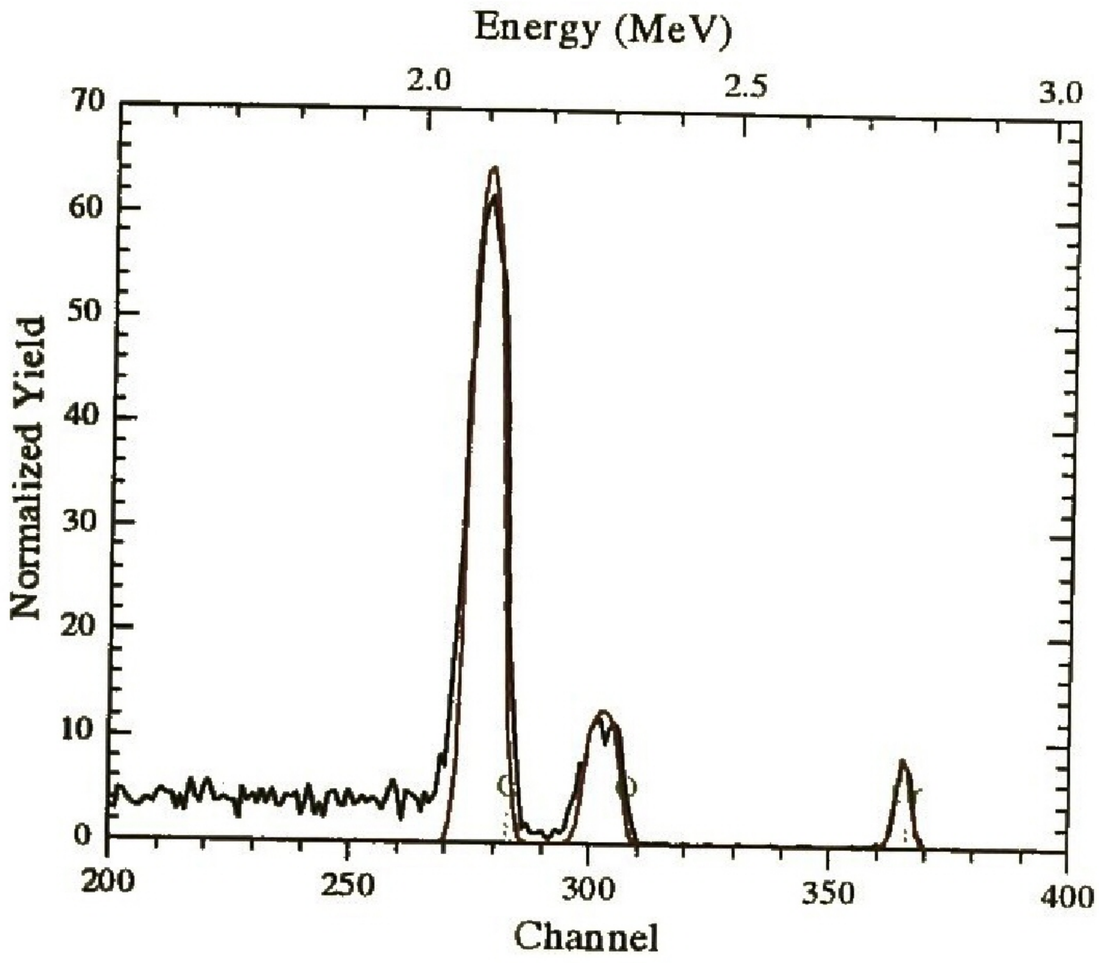

Figure 4.3.(a) Experimental spectrum (Black) and simulation (Red) of Cr/Mylar for 3.0 MeV protons in the NMP chamber

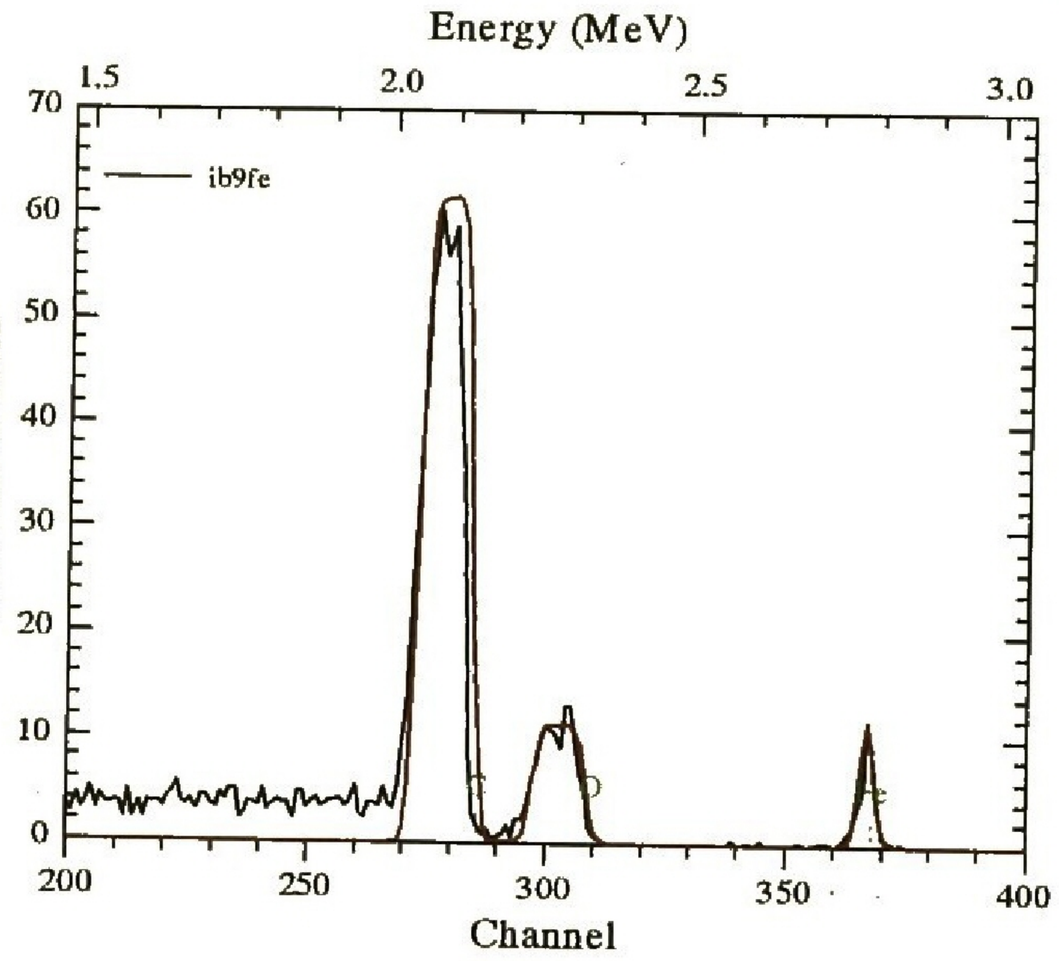

Figure 4.3.(b) Experimental spectrum (Black) and simulation (Red) of Fe/Mylar for 3.0 MeV protons in the NMP chamber

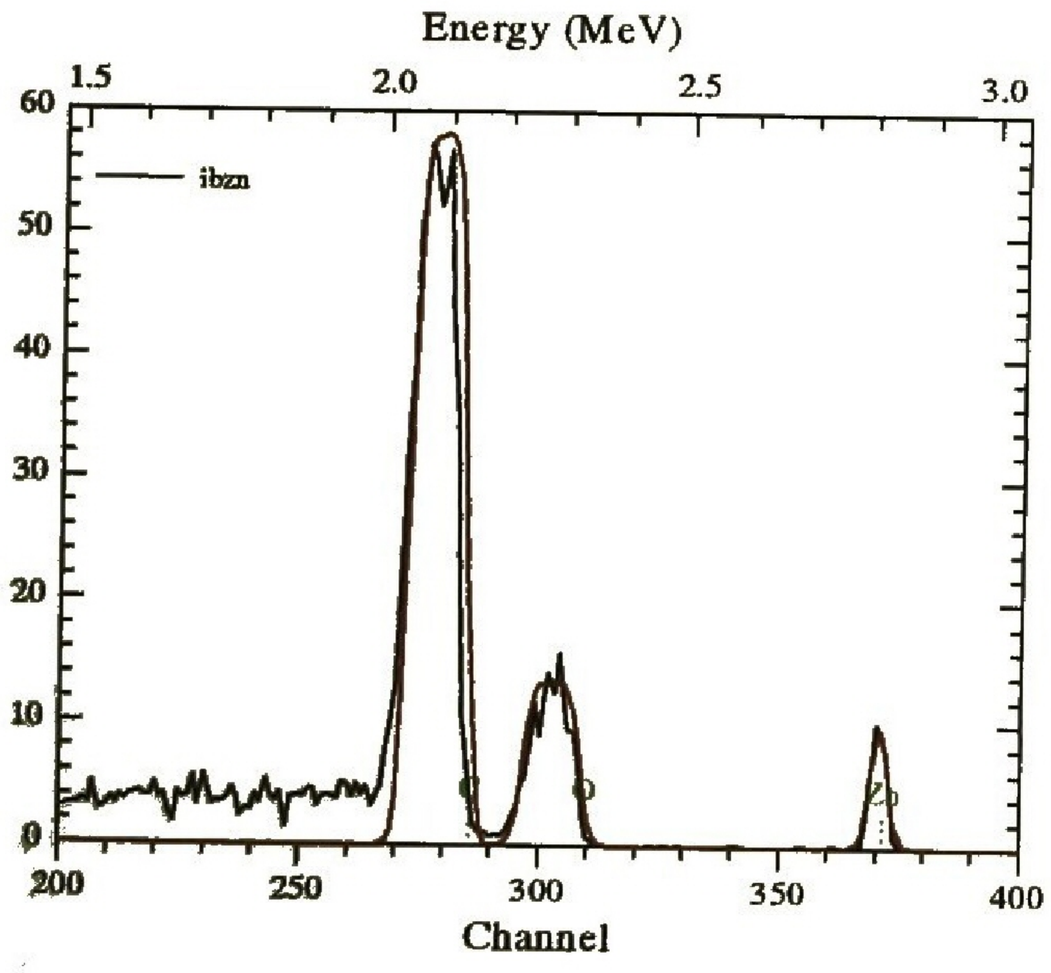

Figure 4.3.(c) Experimental spectrum (Black) and simulation (Red) of Zn/Mylar for 3.0 MeV protons in the NMP chamber

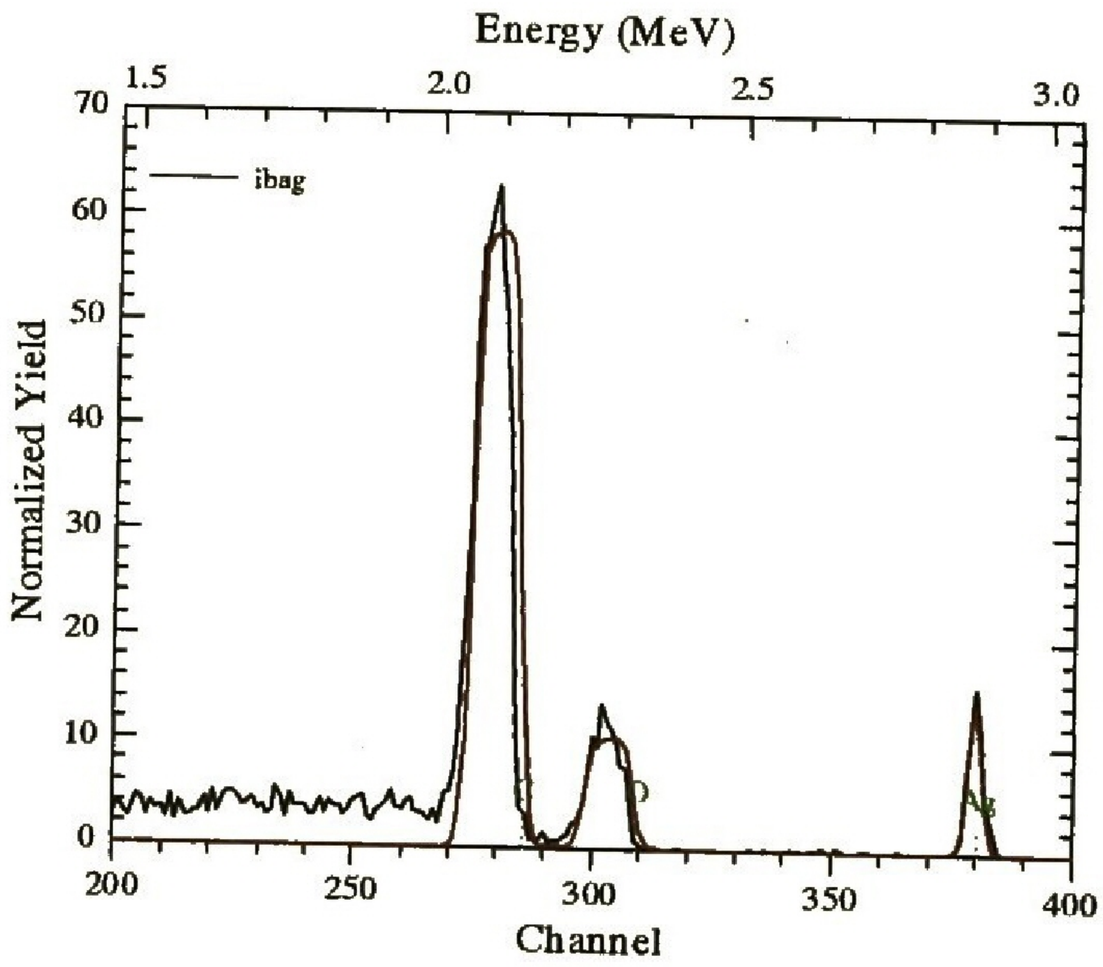

Figure 4.3.(d) Experimental spectrum (Black) and simulation (Red) of Ag/Mylar for 3.0 MeV protons in the NMP chamber

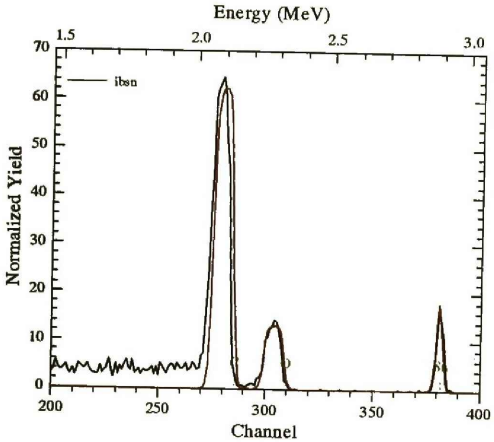

Figure 4.3.(e) Experimental spectrum (Black) and simulation (Red) of Sn/Mylar for 3.0 MeV protons in the NMP chamber

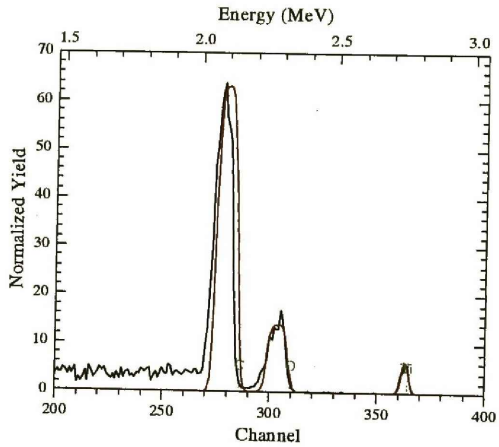

Figure 4.3.(f) Experimental spectrum (Black) and simulation (Red) of Ti/Mylar for 3.0 MeV protons in the NMP chamber

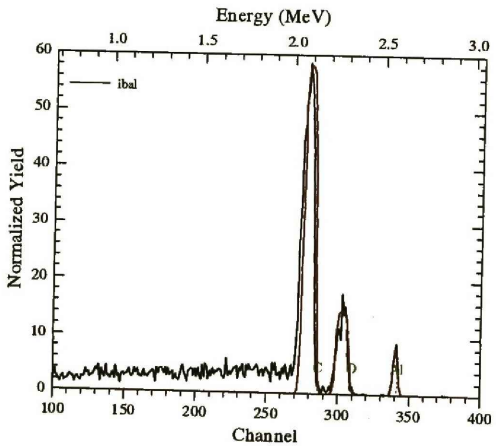

Figure 4.3.(g) Experimental spectrum (Black) and simulation (Red) of Al/Mylar for 3.0 MeV protons in the NMP chamber

4.3.1. Elemental concentration from GeoPIXE

Table 4.9. Results of elemental concentration measurements from GeoPIXE.

Element	Concentration (%) (mass)
Al	Complete absorption
Ti	53.0
Cr	62.8
Fe	63.8
Zn	65.7
Ag	68.0
Sn	77.0

The above concentrations were from all measured elements except aluminum. This was due to the total absorption of aluminum X-rays by the beryllium filter. The concentrations of these elements were expected to be around 100%. However this was not the case. Based on the results, it was concluded that there was a systematic error and also the cross-section for PIXE were not reliable when using 2 MeV alpha particles. The overall conclusion was that the results for GeoPIXE analysis could not be trusted in this particular experiment.

4.4. Comparison of measurements for metal layers on silicon substrate performed in both chambers for 2.0 MeV alpha particles

The figures 4.4 (a-p) show measurements and simulations from both the solid-state and the nuclear microprobe beam lines. The element signal shown in green indicates the position of the different elements if they were on the surface. It can be noticed in figure 4.4.b, 4.4.f, 4.4.j and 4.4.n that the substrate (silicon) and the surface element (aluminum) signals occurred close to one another. The energy difference between the two elements was too small to resolve their peaks hence the elements appeared nearly on the same channel. Figure 4.4.e to 4.4.h and figure 4.4.m to 4.4.p are the measurements and simulations where the matrixes consisted of three elements. The higher peaks are the gold layer and the lower ones are for the surface elements. The silicon peak was not observed in all simulations because it appeared at low energies and on part of the spectra where we were less concerned because it is where multiple scattering plays a very important role. The simulations in figures 4.4.e, 4.4.f, 4.4.m and 4.4.n show slight mismatches. This is because the signals from the surface layer and the substrate were not well resolved. However the overall simulation results showed good agreement.

The same samples were again evaluated with both RUMP and GUPIX. The following tables show the results obtained in both beam lines using the two techniques.

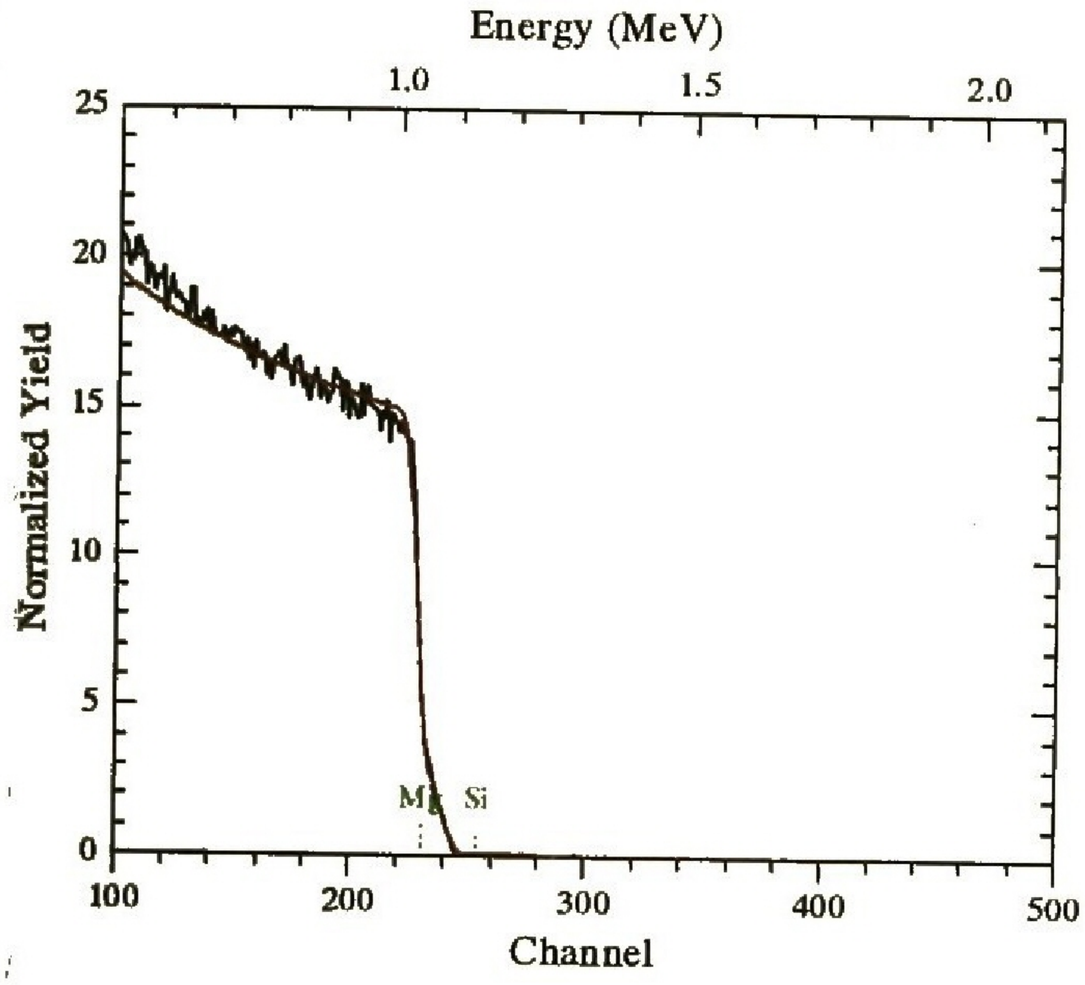

Figure 4.4.(a) Experimental spectrum (Black) and simulation (Red) of Magnesium for 2.0 MeV alpha particles in the SS chamber

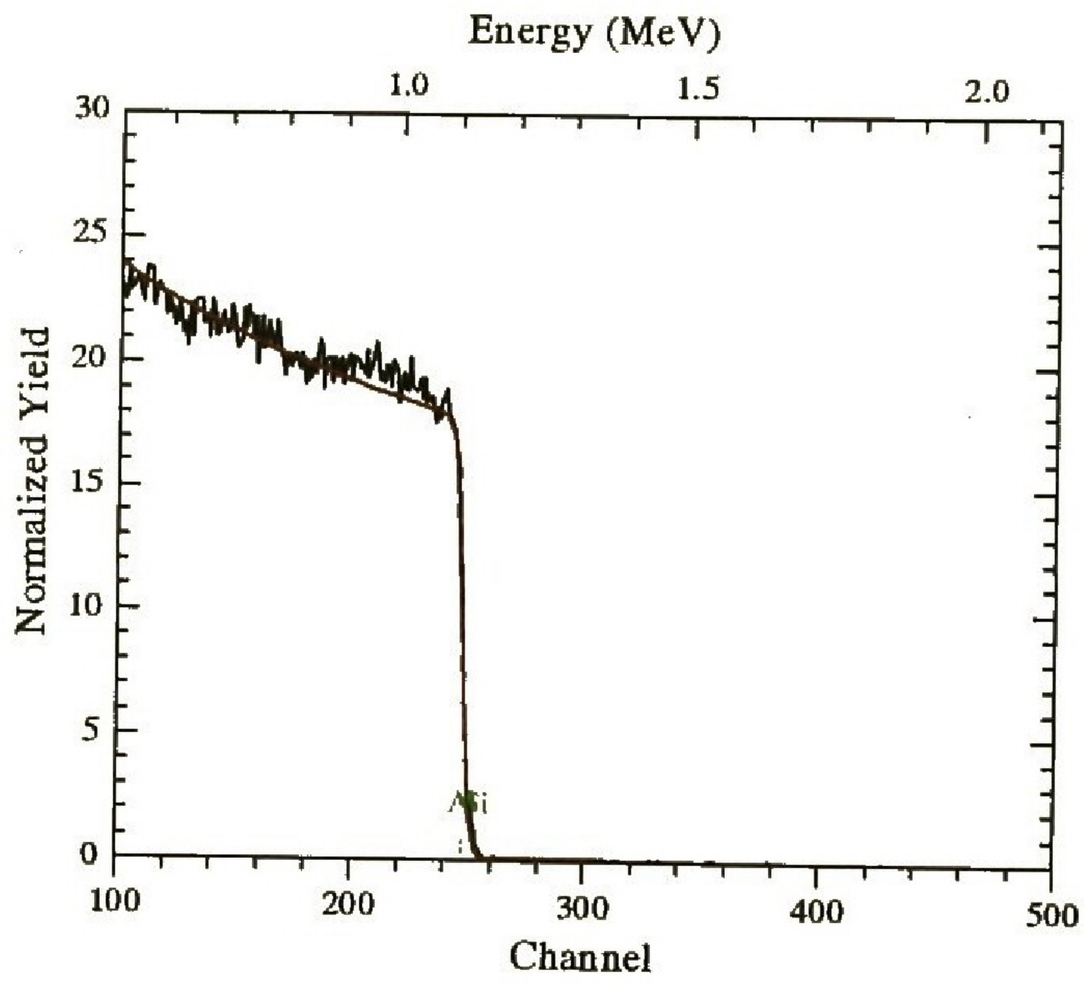

Figure 4.4.(b) Experimental spectrum (Black) and simulation (Red) of Aluminum for 2.0 MeV alpha particles in the SS chamber

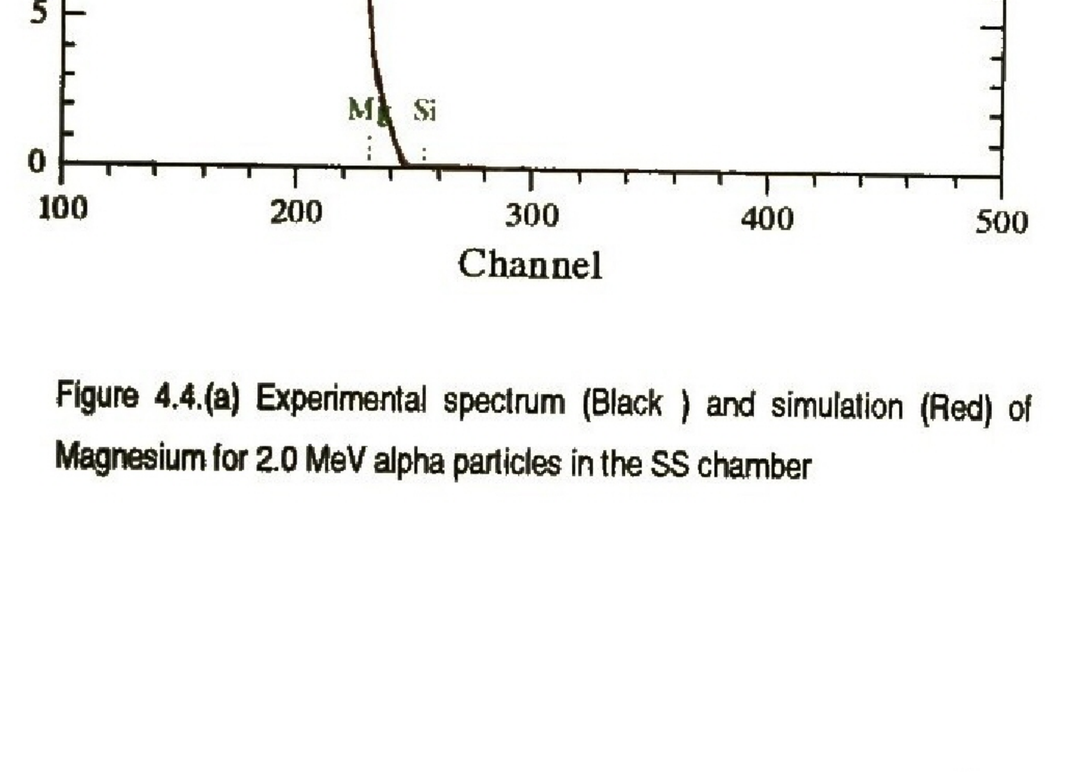

Figure 4.4.(c) Experimental spectrum (Black) and simulation (Red) of Titanium for 2.0 MeV alpha particles in the SS chamber.

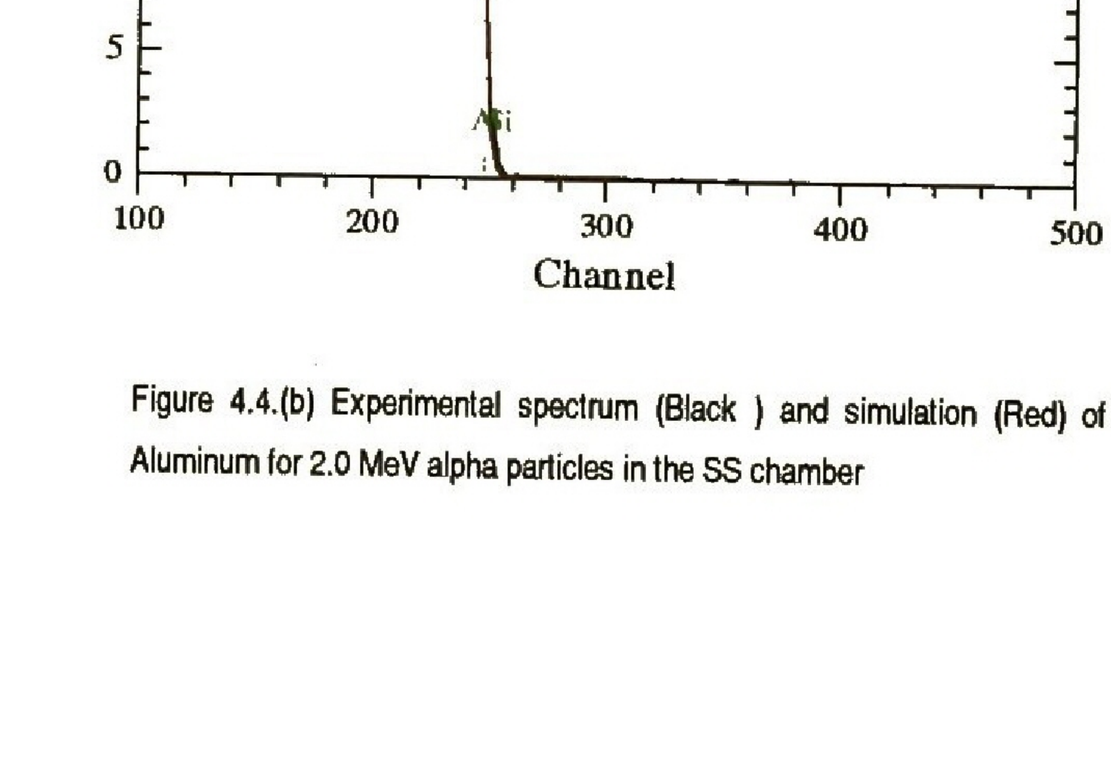

Figure 4.4.(d) Experimental spectrum (Black) and simulation (Red) of Copper for 2.0 MeV alpha particles in the SS chamber.

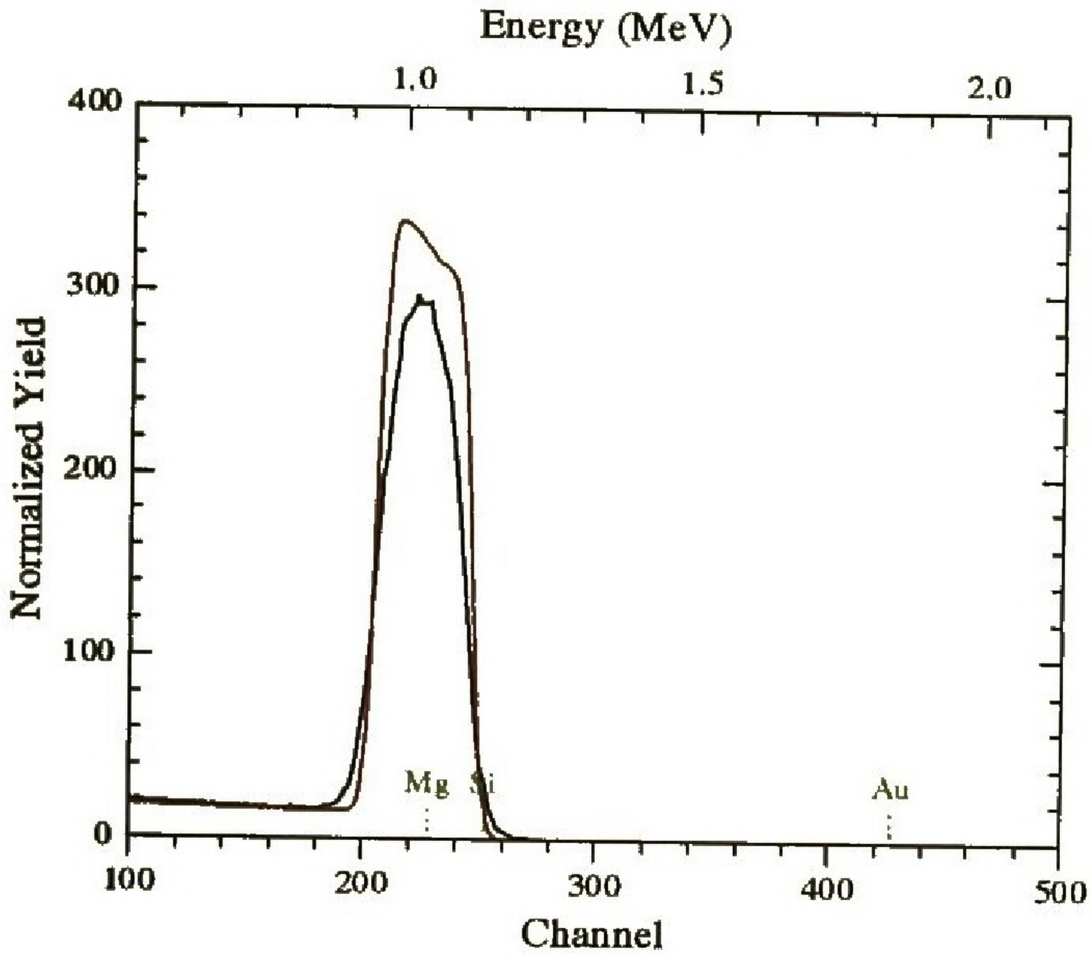

Figure 4.4.(e) Experimental spectrum (Black) and simulation (Red) of **Mg/Au for 2.0 MeV** alpha particles in the SS chamber.

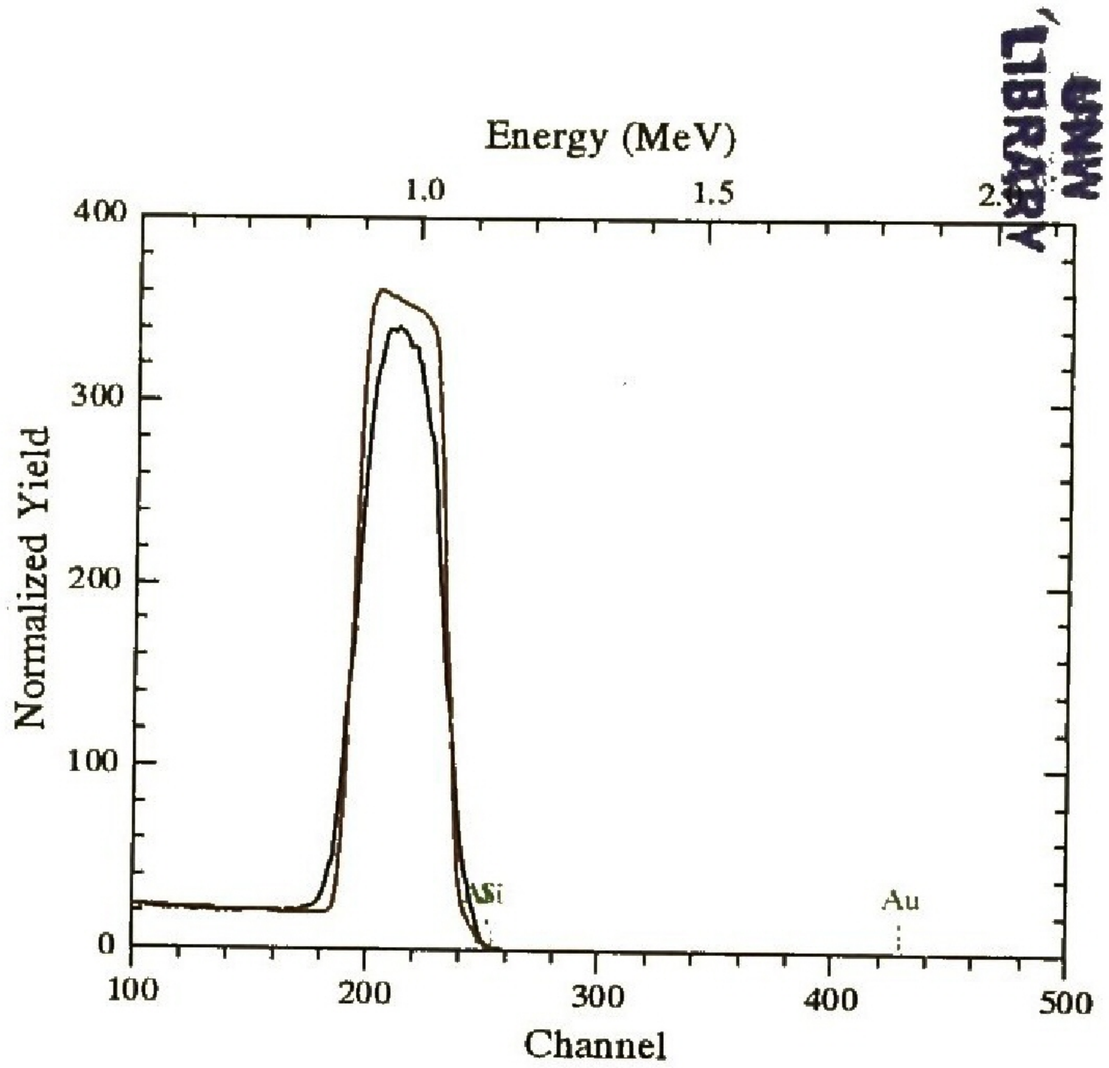

Figure 4.4.(f) Experimental spectrum (Black) and simulation (Red) of Al/Au for 2.0 MeV alpha particles in the SS chamber.

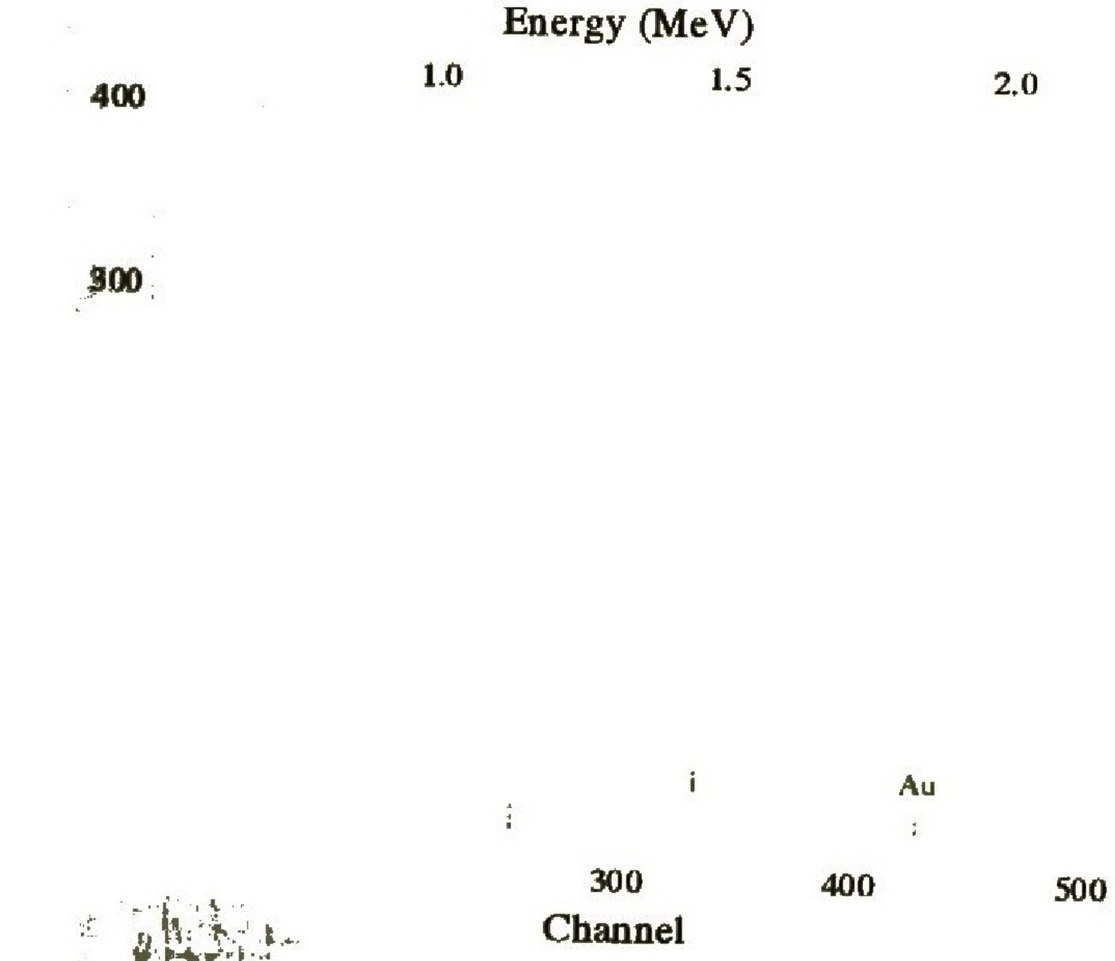

Figure 4.4.(g) Experimental spectrum (Black) and simulation (Red) of **Ti/Au for 2.0 MeV** alpha particles in the SS chamber.

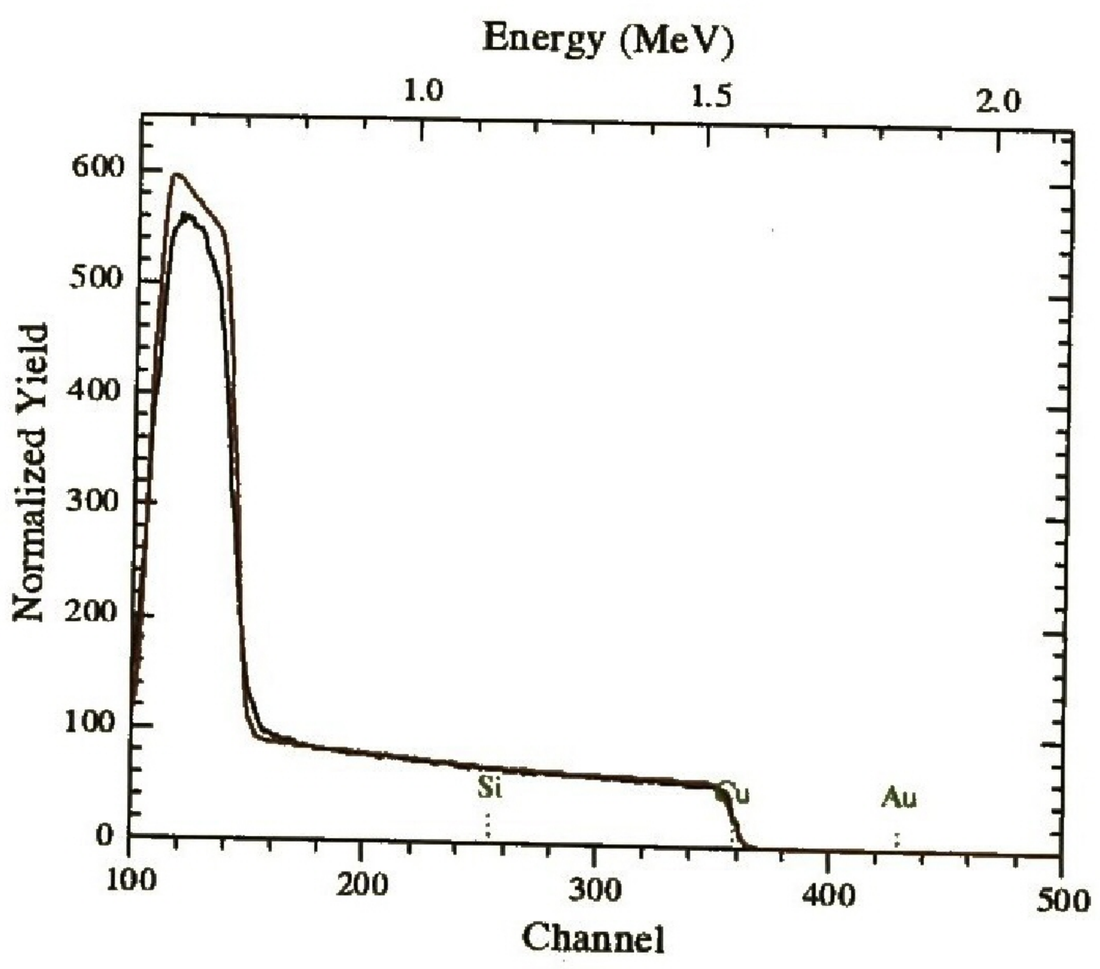

Figure 4.4.(h) Experimental spectrum (Black) and simulation (Red) of Cu/Au for 2.0 MeV alpha particles in the SS chamber.

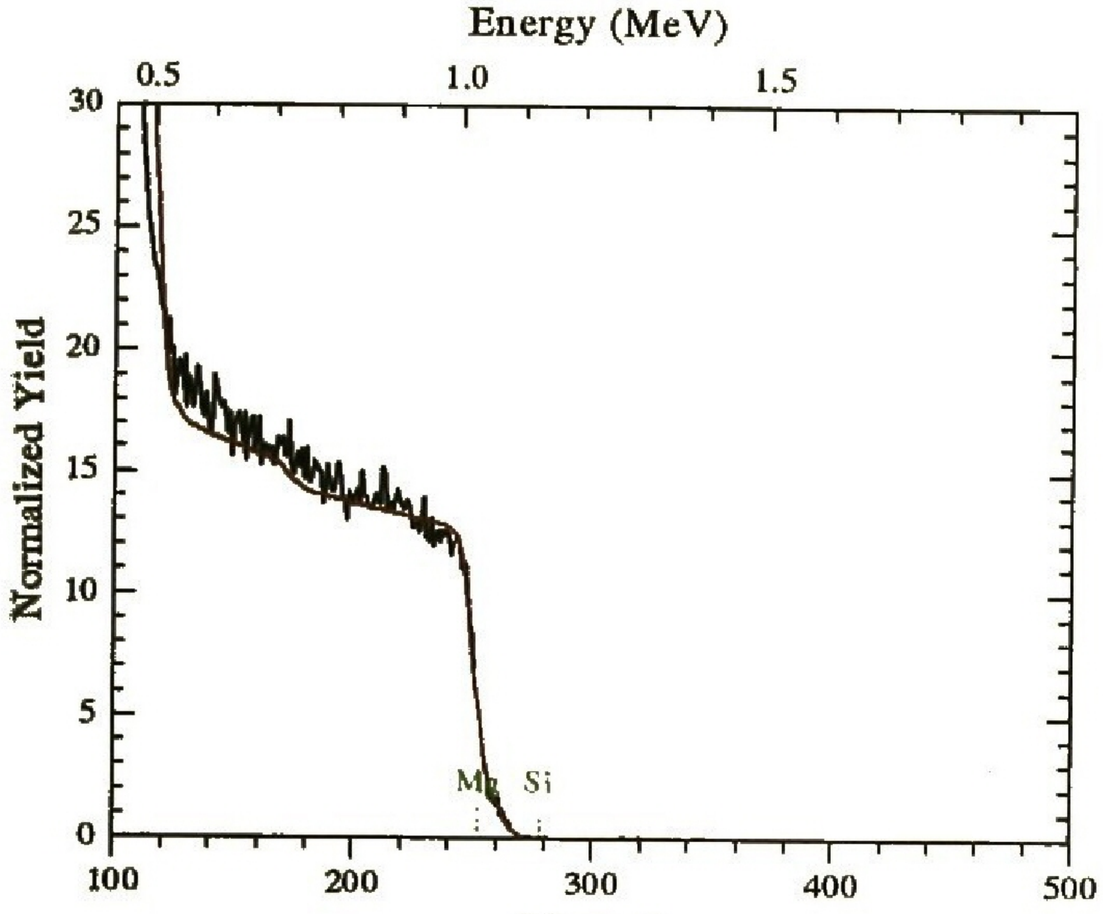

Figure 4.4.(i) Experimental spectrum (Black) and simulation (Red) of Magnesium for 2.0 MeV alpha particles in the NMP chamber.

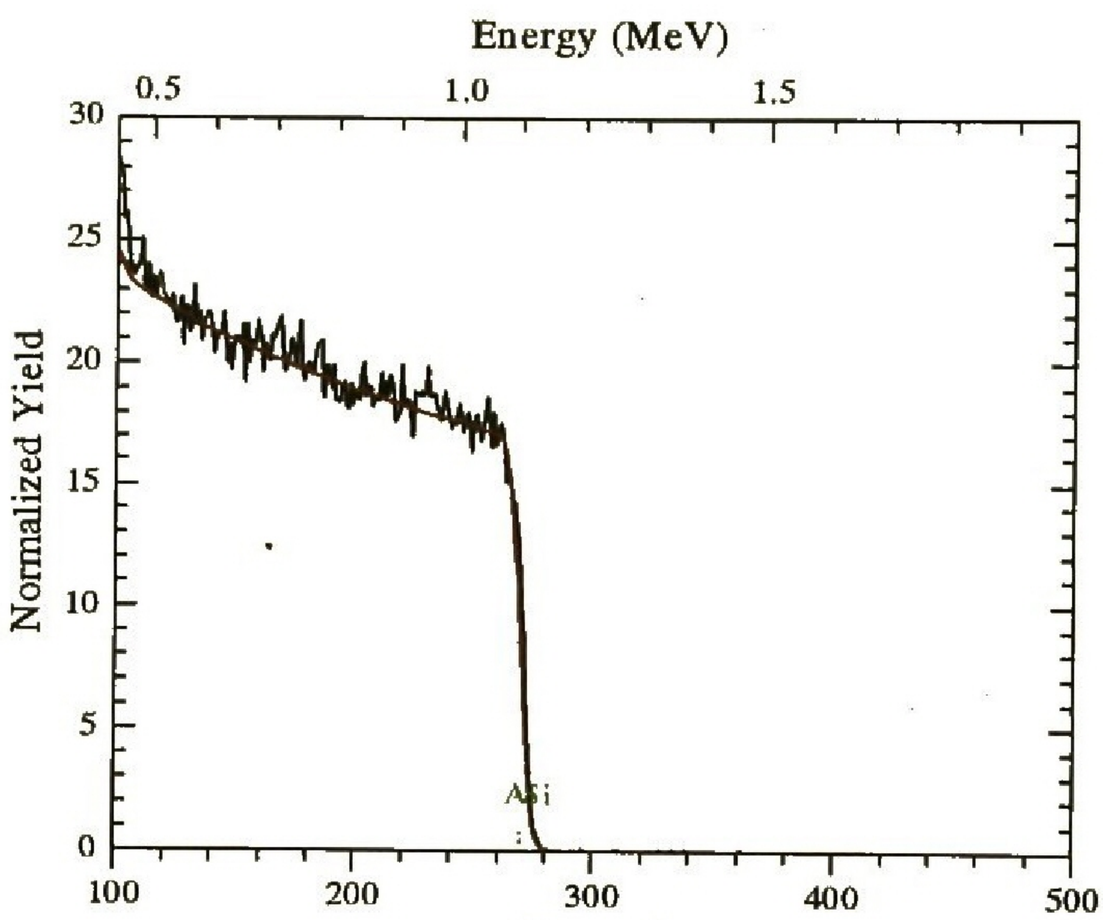

Figure 4.4.(j) Experimental spectrum (Black) and simulation (Red) of Aluminum for 2.0 MeV alpha particles in the NMP chamber.

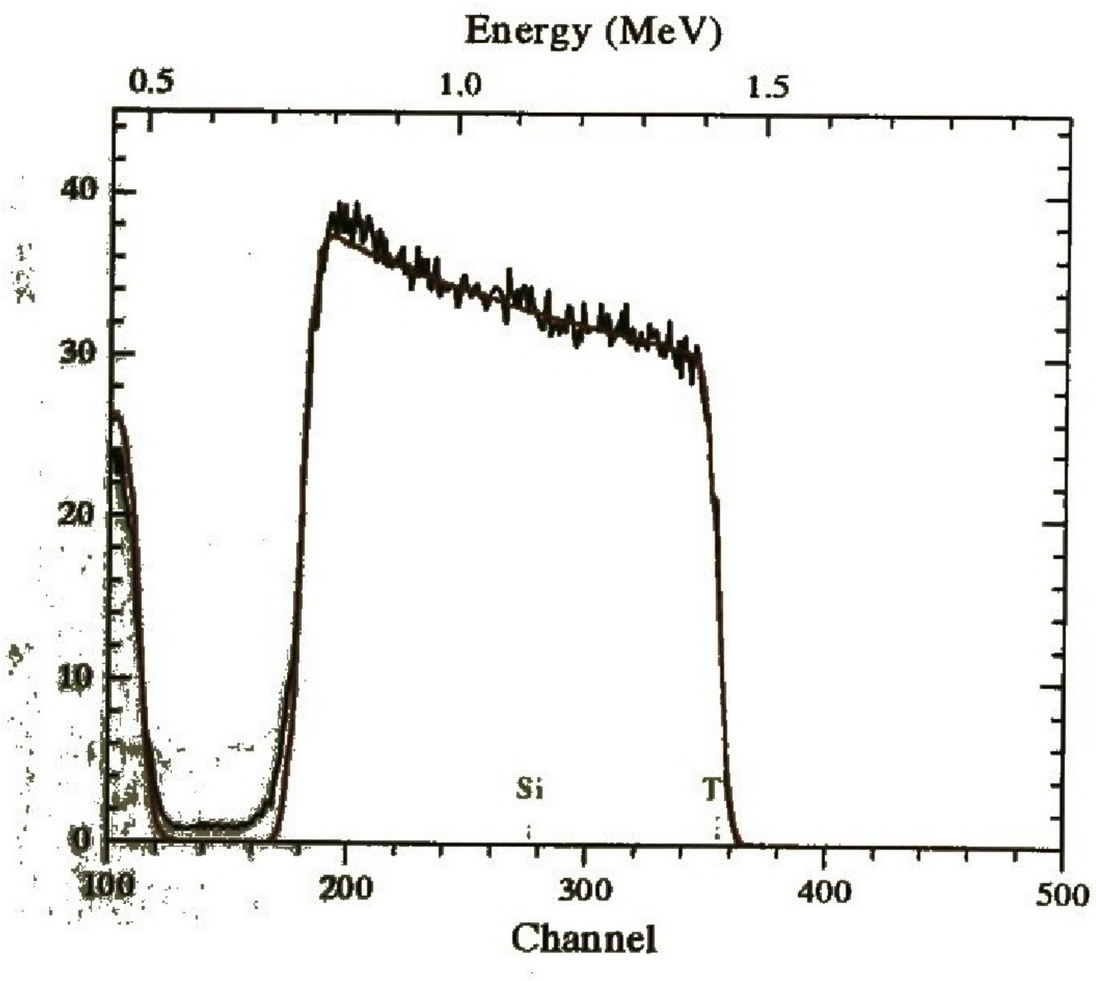

Figure 4.4.(k) Experimental spectrum (Black) and simulation (Red) of Titanium for 2.0 MeV alpha particles in the NMP chamber.

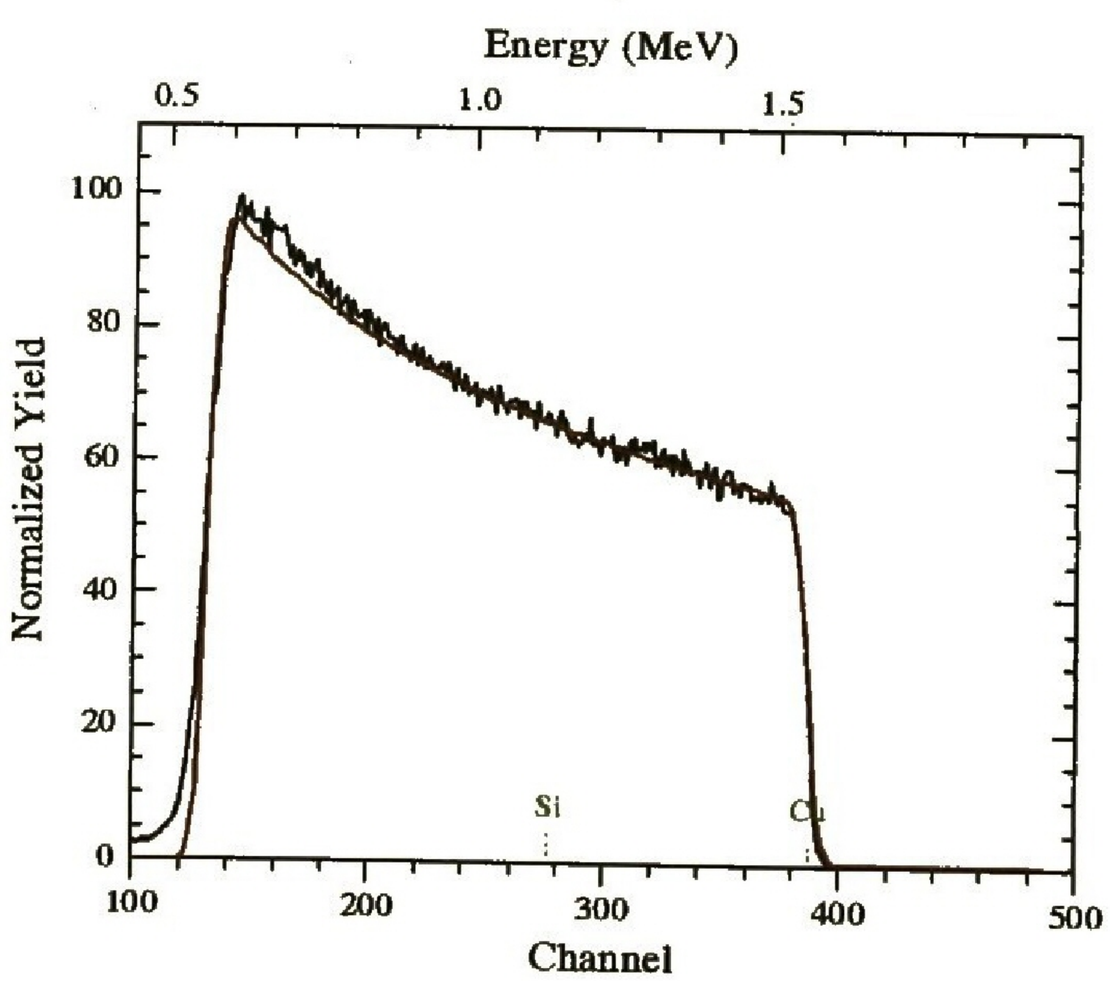

Figure 4.4.(l) Experimental spectrum (Black) and simulation (Red) of Copper for 2.0 MeV alpha particles in the NMP chamber.

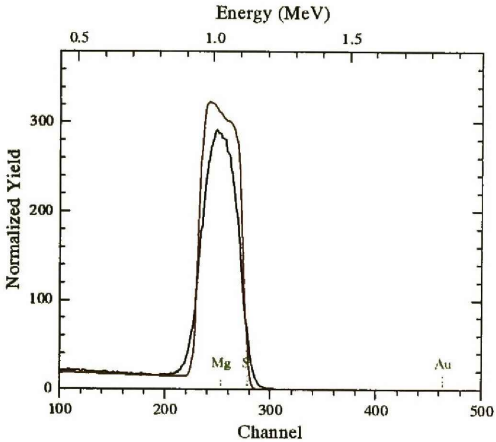

Figure 4.4.(m) Experimental spectrum (Black) and simulation (Red) of Mg/Au for 2.0 MeV alpha particles in the NMP chamber.

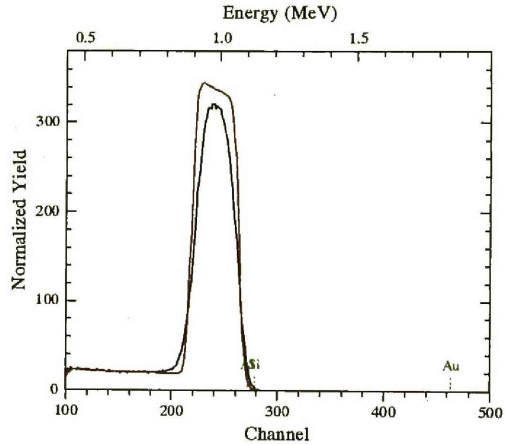

Figure 4.4.(n) Experimental spectrum (Black) and simulation (Red) of Al/Au for 2.0 MeV alpha particles in the NMP chamber.

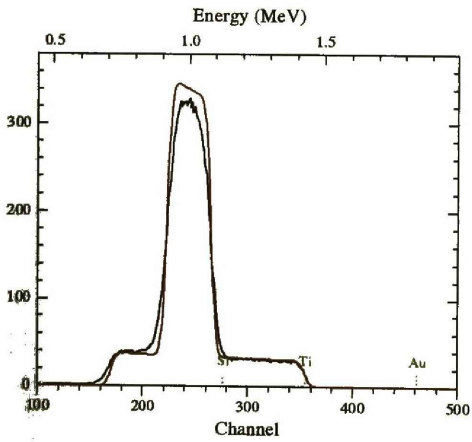

Figure 4.4.(o) Experimental spectrum (Black) and simulation (Red) of Ti/Au for 2.0 MeV alpha particles in the NMP chamber.

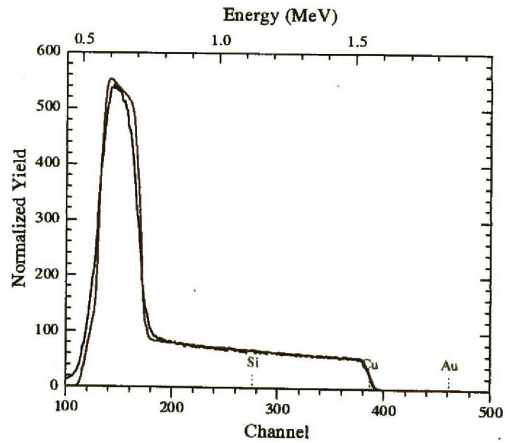

Figure 4.4.(p) Experimental spectrum (Black) and simulation (Red) o Cu/Au for 2.0 MeV alpha particles in the NMP chamber.

Table 4.10. RBS measurements of thin layer metals on silicon and of pure metals on gold on silicon substrate using RUMP at 2.0 MeV alpha particles in the solid-state chamber.

Pure metals on silicon substrate	
Sample	Thickness [mg/cm^2]
Mg/si	0.322
Al/si	0.413
Ti/si	0.409
Cu/si	0.855
Pure metals on gold on silicon substrate	
Mg/au	0.311
Al/au	0.373
Ti/au	0.411
Cu/au	0.859

Thickness measurements for RBS in both beam lines showed good agreement. It can be observed from the table that the values found were close. PIXE results that showed good agreement were the one for copper. Figure s and t shows how the peaks should be resolved in order to get good results. However this was not the case with other elements. The reason we got discrepancies was due to the closeness of the energy peaks hence the detector found it difficult to resolve the peaks of both the substrate and the surface element (figure 4.4. q and r) for magnesium and aluminum. For magnesium and aluminum there was total absorption by the beryllium filter. Titanium results could not be accounted for since it was difficult to get convincing results even when all parameters were correct. It was concluded that the cross-sections of titanium should be reviewed

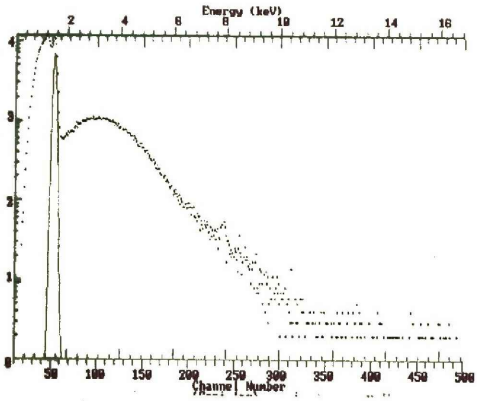

Figure 4.4.(q) Unresolved peaks of aluminum and silicon substrate.

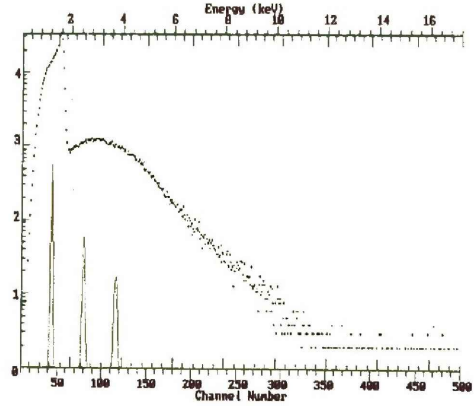

Figure 4.4.(r) Unresolved peaks of magnesium and silicon substrate.

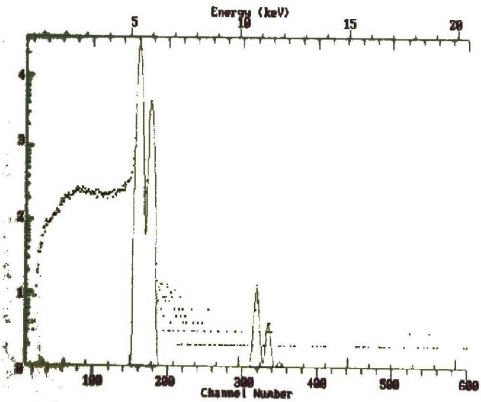

Figure 4.4.(s) Resolved peak of chromium on mylar substrate.

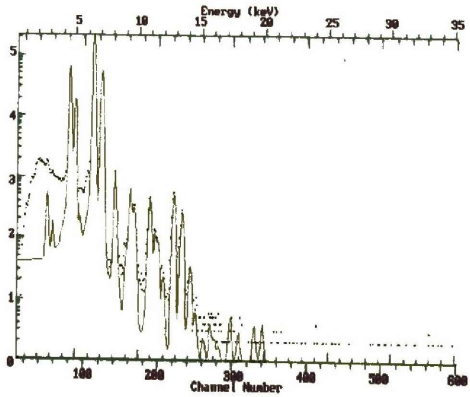

Figure 4.4.(t) Resolved peaks of titanium and tantalum on iron substrate.

Table 4.11. RBS and PIXE measurements of thin layer metals on silicon and of pure metals on gold on silicon substrate using RUMP and GUPIX at 2.0 MeV alpha particles in the nuclear microprobe chamber.

Pure metals on silicon substrate			
Sample	Thickness [mg/cm^2]		
	BS	PIXE [1]	PIXE [2]
Mg/si	0.312	1.49	*
Al/si	0.386	0.012	*
Ti/si	0.386	0.028	0.688
Cu/si	0.806	0.717	1.040
Pure metals on gold on silicon substrate			
	BS	PIXE [1]	PIXE [2]
Mg/au	0.311	0.607	*
Al/au	0.379	0.154	*
Ti/au	0.409	0.275	*
Cu/au	0.852	0.692	*

*** the system (GUPIX) crashes hence no results**

4.4.1. Elemental concentration from GeoPIXE

Table 4.12. Results of elemental concentration measurements from GeoPIXE.

Element	Concentration (%)	Layer thickness from BS [mg/cm^2]
Mg/si	378	0.312
Al/si	44.6	0.386
Ti/si	11.7	0.386
Cu/si	11.6	0.806
Mg/au	11.6	0.311
Al/au	236	0.379
Ti/au	44.6	0.409
Cu/au	58.5	0.852

The elemental concentration for both aluminum and magnesium were considered to be invalid due to the problem of unresolved peaks. That is the X-ray peaks for these two elements are so close to that of the substrate hence the signals from both the substrate and the surface element are taken as one. The other problem was due to the total absorption of the two elements by the beryllium filter. The results for titanium and copper showed less concentration than expected. These results confirmed the problem of GeoPIXE in concentration measurements for this study. The results were considered to be incorrect.

4.5.1. Simulations of thin metal layers on silicon substrate using 3.0 MeV protons in the nuclear microprobe.

The samples used in this experiment were thicker than the ones used in measurements involving 2 MeV alpha particles. The simulations from the samples showed good agreement. The light elements were detected due to that they have lower stopping cross sections and higher scattering cross section for protons. Figure 4.5. b, c, f and g showed some discrepancies in simulations. This was due to the incorrect Rutherford's cross-section for light elements. For this case the elements were aluminum and titanium and their cross sections were too low. The energy difference between copper and gold was found to be small hence the signals from the two elements overlapped to produce a peak and shoulder as shown in figure 4.6(h). The figures also illustrated the fact that heavy elements on a light substrate can be investigated. Thickness determination was then done based on the simulations. The following tables show the comparison between RBS and PIXE for layer thickness evaluation from the samples and standards.

Table 4.13. RBS and PIXE measurements of thin layer metals on silicon substrate using RUMP and GUPIX at 3.0 MeV protons in the nuclear microprobe chamber.

Pure metals on silicon substrate				
Sample	Thickness [mg/cm^2]			
	BS	PIXE [1]	Thin layer	Thick layer
Mg/si	0.279	7.065	34.064	0.000
Al/si	0.179	0.265	1.794	4.388
Ti/si	0.493	0.411	0.401	0.417
Cu/si	0.949	0.948	0.901	0.948
Pure metals on gold on silicon substrate				
	BS	PIXE [1]	Thin layer	Thick layer
Mg/au	0.380	0.000	0.000	0.000
Al/au	0.506	0.132	0.000	0.000
Ti/au	0.460	0.448	0.451	0.433
Cu/au	1.003	1.005	0.948	0.901

From the above tables it was observed that option number two of PIXE was not applicable. However the software is also equipped with options whereby one can specify whether the layer is thick or thin. These two options were used. The results showed good agreement for titanium and copper. For magnesium and aluminum the results did not match and as discussed earlier it was concluded that either the detector could not differentiate between the counts from the substrate and the surface element (figure 4.4. q-r). The conclusion from copper and titanium results was that PIXE has demonstrated its ability to measure surface layer thickness.

4.5.3. Elemental concentration from GeoPIXE

Table 4.14. Results of elemental concentration measurements from GeoPIXE.

Element	Concentration (%)	Layer thickness from BS [mg/cm^2]
Mg/si		0.279
Al/si		0.179
Ti/si	85.9	0.493
Cu/si	80.9	0.949
Mg/au		0.380
Al/au		0.506
Ti/au	83.0	0.460
Cu/au	77.4	1.003

The magnesium and aluminum results were not obtained due to difficulty in peak resolving between the surface element and substrate. The titanium and copper results were found to be around 80%. The results were considered to be incorrect since these were pure elements hence their concentration were expected to be around 100%. The conclusion was that the software found it difficult to give proper results. The results were considered invalid.

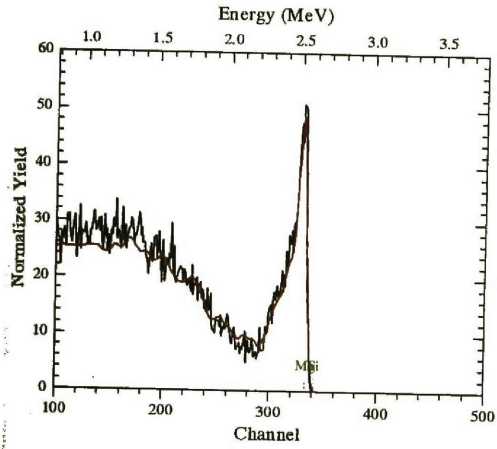

Figure 4.5.(a) Experimental spectrum (Black) and simulation (Red) of Mg for 3.0 MeV protons in the NMP chamber

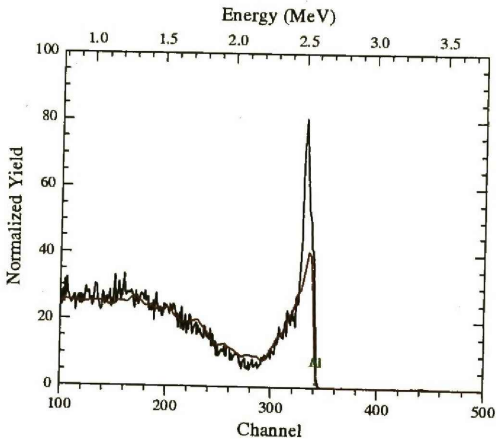

Figure 4.5.(b) Experimental spectrum (Black) and simulation (Red) of Al for 3.0 MeV protons in the NMP chamber

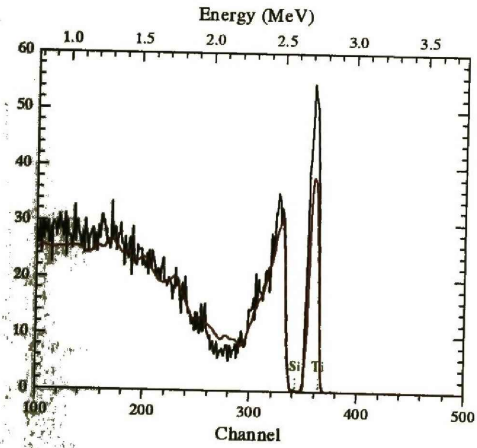

mental spectrum (Black) and simulation (Red) of Ti
protons in the NMP chamber

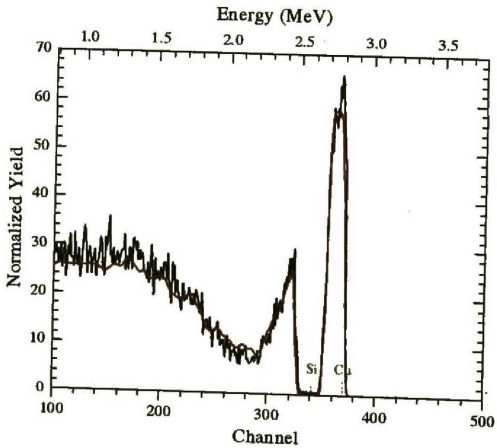

Figure 4.5.(d) Experimental spectrum (Black) and simulation (Red) of Cu for 3.0 MeV protons in the NMP chamber

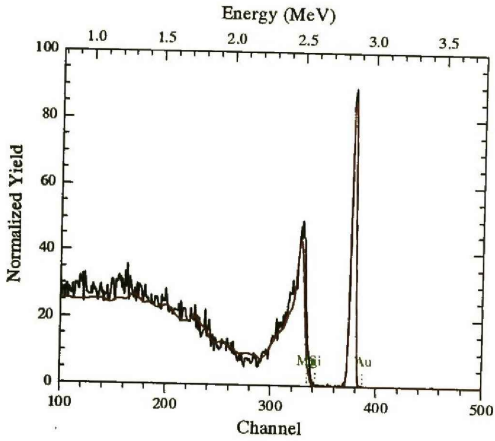

Figure 4.5.(e) Experimental spectrum (Black) and simulation (Red) of Mg/Au for 3.0 MeV protons in the NMP chamber

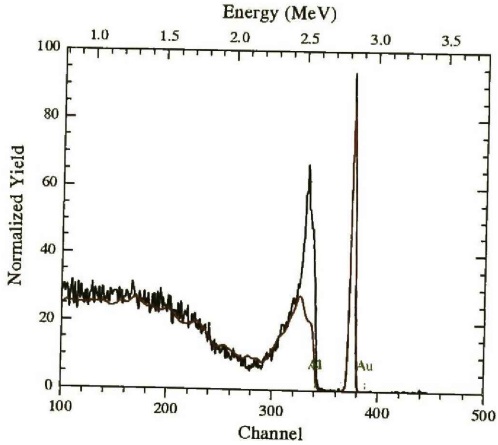

Figure 4.5.(f) Experimental spectrum (Black) and simulation (Red) of Al/Au for 3.0 MeV protons in the NMP chamber

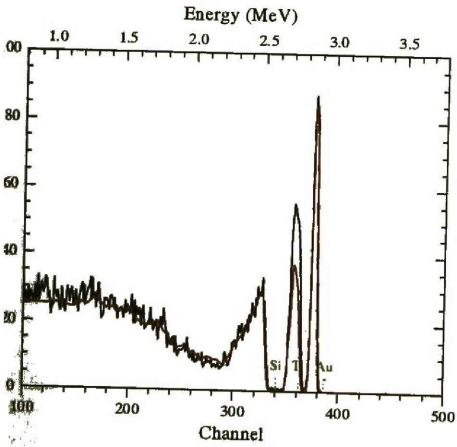

gure 4.5.(g) Experimental spectrum (Black) and simulation (Red) of 3.0 MeV protons in the NMP chamber

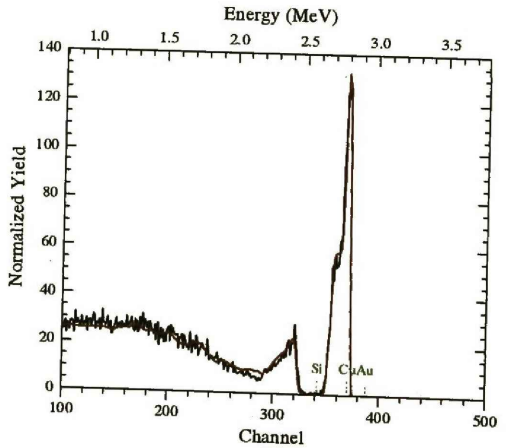

Figure 4.5.(h) Experimental spectrum (Black) and simulation (Red) of Cu/Au for 3.0 MeV protons in the NMP chamber

Chapter 5

5.1. Summary

The study's main objective was to optimize the thickness assessment of surface layers based on the most suitable analytical conditions at the Material Research Group (MRG), iThemba LABS experimental facilities. PIXE in conjunction with backscattering spectrometry were evaluated as a means of thickness measurement with much emphasis on PIXE. The two methods were compared using the published work by Campbell *et al* as reference. The samples were prepared through physical vapor deposition system at iThemba LABS and the MicroMatter™ standards were also analyzed. Computer simulations of RBS spectra were done using software program RUMP. The simulations were done to optimize the thickness of the different layers deposited on the substrates. PIXE spectra were analyzed using software programs GUPIX and Geo-PIXE.

The TiN sample simulations from the publication were found to be of different thickness with sample D-1 being the thinner and D-6 the thicker. This was also found to be the case in this study when 2.5 MeV protons were used (see Fig. 4.2 e-g). The figures showed that light elements on heavy substrate could be detected. The results also showed that protons can penetrate several micrometers into the sample and this is due to their stopping powers. This was confirmed by the results from table 4.7 and 4.8. The values found were closer to the ones from published work since the error was less than 12 %. The results led to the conclusion that PIXE has the ability to measure thickness.

However this was not the case when energies of 2.0 MeV alpha particles were used in both the solid-state (see fig. 4.1 e-g) and the nuclear microprobe (see fig. 4.1 l-n) chambers. The simulations only fitted to a certain limited thickness and the beam-induced electrons resulted in high correction factors. The correct thickness was found on sample D-1 as recorded in table 4.3, 4.4 and 4.6. The tables also showed that the alpha particles were limited to a certain thickness range. It was also observed that RBS has low sensitivity for light elements when using alpha particles. This was confirmed by the nitrogen signal that was submerged in the background produced by titanium. The overall conclusions for the 2.0 MeV alpha particles were that higher energies are to be used. Again the pile-up rejection system needs to be installed in the nuclear microprobe chamber. Hence it was used in the last sessions of the experiments.

The thickness evaluation from own samples showed good simulations. Slight problems were encountered where the detectors found it difficult to resolve signals from both the substrate and the element. This was due to that the energy peaks were so close to one another and were appearing nearly on the same peak. The results for thickness measurement showed consistency for RBS in both chambers. For PIXE the results were only found on copper. This led to the conclusion that the detector resolution needs to be reviewed since it found it not easy to differentiate between signals that lie close to one another.

Simulation with 3.0 MeV protons in both prepared samples and MicroMatter™ standards showed good agreement. In both techniques the corresponding thickness

measurements were on titanium and copper samples (table 4.19 and 4.20). As discussed there was a problem with peak resolving between the substrate (silicon) and the elements (magnesium and aluminum) and this were related to high absorption. It was concluded that the detector resolution was not good enough in the case of PIXE. The MicroMatter™ results were found to be acceptable for BS whereas PIXE results were different from the expected ones. This was confirmed by the difference in error thickness between the two techniques when compared with the certified measurements. The GeoPIXE results were totally different from what was expected. The results were considered to be invalid for this particular study. The conclusion was that the GeoPIXE software could not be trusted for elemental concentration measurements.

5.2. Conclusions

- The investigation of thickness measurement using PIXE, in this study indicated that PIXE is capable of measuring thickness independently.
- The study has proved that PIXE can provide information on the sequence of layers in the material and if the composition is known then it is possible to deduce layer depths with accuracy.
- Data obtained from various experiments shows that PIXE can give accurate measurements.
- The study also showed that the detector resolution needs to be reviewed and that more work is to be done on cross section measurements of different elements especially the light ones.

- GeoPIXE has failed to give correct results for elemental concentration except for TiN at 2.5 MeV protons.
- The beam on-demand pulsing system is significant in the nuclear microprobe chamber because it results in the integration of correct charge measurements.
- The overall conclusion from the study was that the thickness assessment of surface layers based on the most suitable analytical conditions at the Material Research Group (MRG), iThemba LABS experimental facilities has been correctly optimized.

References

M. Ahmed, M. Faiz, M.A. Al-Ohali and O. Fageeha, Depth profiling of a single crystal of YBCO superconductor using micro-PIXE technique, Nucl. Instr. and Meth. in Phys. Research B 132 (1997) 507-512.

R. Amirikas, D.N. Jamieson and S.P. Dooley, Measurement of (p, p) elastic cross sections for C, O and Si in the energy range 1.0-3.5 MeV, Nucl. Instr. and Meth. in Phys. Research B 77 (1993) 110-116.

G. Amsel, E. Girard, G. Vizkelethy, G. Battistig, Y. Girard and E. Szilágyi, High pulse rate and pileup handling in precision RBS, Nucl. Instr. and Meth. in Phys. Research B 64 (1992) 811-816

M.B.H. Breese, D.N. Jamieson, P.J.C. King, Material Analysis Using Nuclear Microprobe, (1996), John Wiley & Sons.

I. Brissaud, J. Frontier and P. Regnier, Evaluation of depth profiling with PIXE, Nucl. Instr. and Meth. in Phys. Research B 12 (1985) 235-244

J.L. Campbell and J.A Cookson, PIXE analysis of thick targets, Nucl. Instr. and Meth. in Phys. Research B 3 (1984) 185-197.

J.L. Campbell, T.L. Hopman, J.A. Maxwell and Z. Nejedly, The Guelph PIXE software package III: Alternative proton database, Nucl. Instr. and Meth. in Phys. Research B 170 (2000) 193-204.

J.L. Campbell, W.J. Teesdale, J.A. Maxwell and V.M. Prozesky, Thickness measurement of titanium nitride layers on steel using PIXE and proton backscattering, Nucl. Instr. and Meth. in Phys. Research B 85 (1994) 108-111.

C.L. Churms, J.V. Pilcher, K.A. Springhorn and U.A.S. Tapper, A VAX and PC-based data acquisition system for MCA, scanning and list-mode analysis, Nucl. Instr. and Meth. in Phys. Research B 77 (1993) 56-61.

A. Climent-Font, U. Wätjen and H. Bax, Quantitative RBS analyzing RUMP on the accuracy of the He stopping in Si, Nucl. Instr. and Meth. in Phys. Research B 71 (1992) 81-86

G. Demortier, S. Mathot and B. Van Oystaeyen, Complementarity of RBS, PIGE and PIXE for the determination of surface layers of thickness up to 30 microns, Nucl. Instr. and Meth. in Phys. Research B 49 (1990) 46-51.

L.R. Doolittle, A semiautomatic algorithm for Rutherford backscattering analysis, Nucl. Instr. and Meth. in Phys. Research B 15 (1986) 227-231.

L.C. Feldman and J.W. Mayer, Fundamental of Surface and Thin Film Analysis, (Elsevier Press, 1986).

V. Havranek, V. Hnatowicz, J. Kvitek, J. Musil and V. Poulek, Determination of nitrogen content in thick TiN layers by proton backscattering, Nucl. Instr. and Meth. in Phys. Research B 47 (1990) 433-438.

M. Jakšić, M. Vajić, S. Fazinić, D. Rendić, T. Tadić and V. Valković, PIXE Depth Profiling, Nucl. Instr. and Meth. in Phys. Research B 40/41 (1989), 643-645.

S.A.E. Johansson, J.L. Campbell and K.G. Malmqvist, PIXE, (1995), John Wiley & Sons.

J.A. Maxwell, J.L. Campbell and W.J. Teesdale, The Guelph PIXE package, Nucl. Instr. and Meth. in Phys. Research B 43 (1989) 218-230.

J.A. Maxwell, W.J. Teesdale and J.L. Campbell, The Guelph PIXE software package II, Nucl. Instr. and Meth. in Phys. Research B 95 (1995) 407-421

T. Osipowicz, T. Corts, K. Lieb and F.Bergmeister, PIXE measurement of Kr-sputted TiN coatings, Nucl. Instr. and Meth. in Phys. Research B 50 (1990) 238-242.

V.M. Prozesky, W.J. Przybylowicz, E. van Achterbergh, C.L. Churms, C.A. Pineda, K.A. Springhorn, J.V. Pilcher, C.G. Ryan, J. Kritzinger, H. Schmitt and T. Swart, The

NAC nuclear microprobe facility, Nucl. Instr. and Meth. in Phys. Research B 104 (1995) 36-42.

W.J. Przybylowicz, J. Mesjasz-Przybylowicz, C.A. Pineda, C.L. Churms, K.A. Springhorn and V.M. Prozesky, Biological applications of the NAC nuclear microprobe, X-ray Spectrum. 28 (1999) 237-243.

J. Räisänen, Experimental arrangements for the simultaneous use of PIXE and complementary accelerator based techniques, Nucl. Instr. and Meth. in Phys. Research B 49 (1990) 39-45.

A.R. Ramos, A. Paúl, L. Rijniers, M.F. da Silva and J.C. Soares, Measurement of (p,p) elastic differential cross-sections for carbon, nitrogen, oxygen, aluminium and silicon in the 500-2500 keV range at 140^0 and 178^0 laboratory scattering angles, Nucl. Instr. and Meth. in Phys. Research B 190 (2002) 95-99.

RUMP Manual, November 1996

C.G. Ryan, Quantitative trace element imaging using PIXE and the nuclear microprobe, International Journal of Imaging Systems and Technology, (2001).

C.G. Ryan, D.R. Cousens, S.H. Sie and W.L. Griffin, Quantitative analysis of PIXE spectra in Geoscience applications, Nucl. Instr. and Meth. in Phys. Research B 49 (1990(b)) 271-276.

C.G. Ryan, D.R. Cousens, S.H. Sie, W.L. Griffin, G.F. Suter and E. Clayton, Quantitative PIXE microanalysis of geological material using the CSIRO proton microprobe, Nucl. Instr. and Meth. in Phys. Research B 47 (1990) 55-71.

C.G. Ryan and E. van Achterbergh, A comparison of H+ and H2+ beams for quantitative PIXE microanalysis, NAC (National Accelerator Centre) Annual Report, (March, 1993), NAC/AR/93-01, p. 39.

C.G. Ryan, E. van Achterbergh, C.J. Yeats, T.T. Win and C. Cripps, Quantitative PIXE trace element imaging of minerals using the new CSIRO-GEMOC nuclear microprobe, Nucl. Instr. and Meth. in Phys. Research B 189 (2002) 400-407.

U.A.S.Tapper, W.J. Przybylowicz and H.J. Annegarn, Chemical Analysis by Nuclear Method 'Particle-Induced X-ray Emission", (John Wiley and Sons, 1994).

G. Vizkelethy, Computer simulation of ion beam methods in analysis of thin films, Nucl. Instr. and Meth. in Phys. Research B 89 (1994) 122-130.

F. Watt and G.W. Grime, Principles and Applications of high-energy ion beams, IOP Publishing Ltd, 1987.

WEB page references:

www.microscopyu.com

www.nanoscience.com

www.rit.edu/%7Ebekpph/sem/572_outline.html